Mapping Plant Communities in the Intertidal Zones of the Yellow River Delta Using Sentinel-2 Optical and Sentinel-1 SAR Time Series Data

YANSHA LUO
February 2018

SUPERVISORS:
Dr. Tiejun Wang
Prof. Dr. Xinhui Liu

Mapping Plant Communities in the Intertidal Zones of the Yellow River Delta Using Sentinel-2 Optical and Sentinel-1 SAR Time Series Data

YANSHA LUO
Enschede, The Netherlands, February 2018

Thesis submitted to the Faculty of Geo-Information Science and Earth Observation of the University of Twente in partial fulfilment of the requirements for the degree of Master of Science in Geo-Information Science and Earth Observation.
Specialization: Natural Resource Management

SUPERVISORS:
Dr. Tiejun Wang (University of Twente)
Prof. Dr. Xinhui Liu (Beijing Normal University)
ADVISOR:
Dr. Yiwen Sun (University of Twente)

THESIS ASSESSMENT BOARD:
Dr. Yousif Hussin (Chair, University of Twente)
Dr. Zoltan Vekerdy (External examiner, University of Twente)
Dr. Tiejun Wang (University of Twente)
Prof. Dr. Xinhui Liu (Beijing Normal University)

ABSTRACT

Classification and mapping of the intertidal vegetation play a critical role in wetland conservation planning and policy. Serving as the early indicator of wetland degradation, plant communities in the intertidal zone are the most critical ecological variable in wetland assessment. Traditional survey methods are expensive and time-consuming. With the development of remote sensing techniques, optical satellite images become more popular and efficient compared with field survey. However, the quality of optical images would be influenced by clouds and weather. Thus weather-independent SAR data is considered to provide complementary information for mapping intertidal plant communities. Vegetation indices derived from optical time series data play a crucial role in characterising vegetation phenology. In this study, the intertidal plant communities of the Yellow River Delta were classified using random forest algorithm based on Sentinel-1 and Sentinel-2 time series images as well as the NDVI statistic parameters derived from Sentinel-2 time series. The variable importance of different input data from various classification scenarios was also evaluated. It was found that a high mapping accuracy for the intertidal plant communities was achieved with an overall mapping accuracy of 75.7% and the Kappa coefficient of 0.73 when integrating the Sentinel-2 time series images with its associated NDVI statistic parameters, which is significantly higher than the mapping accuracies derived from either the single-date Sentinel-2 images, Sentinel-1 SAR time series images or the NDVI statistic parameters alone. Besides, when combining Sentinel-1 time series, Sentinel-2 time series and NDVI statistic parameters, a further improved mapping accuracy was achieved with an overall mapping accuracy of 77.7% and the Kappa coefficient of 0.75. The research also showed that autumn image and the red edge bands are the most critical variables for mapping intertidal plant communities. The study suggests that combining the Sentinel-2 optical images with the Sentinel-1 SAR images makes it possible to map intertidal plant communities in a dynamic ecosystem successfully, and with higher accuracy than when using either the Sentinel-2 time series or the Sentinel-1 time series.

Key words: intertidal zones, plant communities, Sentinel-1, Sentinel-2, random forest

ACKNOWLEDGEMENTS

This thesis is the culmination of being a student for 12-month in the faculty of Geo-Information Science and Earth Observation (ITC) of the University of Twente, which entirely expanded my horizons, broadened and deepened my knowledge since I am a green hand without any remote sensing and geographic background. At the time of the ending of my MSc in ITC, I appreciate the opportunity of studying in the joint program of ITC faculty and Beijing Normal University. Here, I would like to express my sincere appreciation to all the people who helped and supported me during the research.

First and foremost, I gratefully acknowledge the guidance of my first supervisor Dr. Tiejun Wang, for introducing me such a fantastic and magic remote sensing world and teaching me how to conduct scientific research independently. I benefited a lot from your patience, perseverance and passion to the scientific research and I appreciate for your advice and encouragement during every discussion and talk, especially after I went back to China. And also thank you very much for suggestions for my difficulties both in study and life, I think some of your advice I will follow and treasure for my lifetime.

My special appreciation to Prof. Dr. Xinhui Liu, my second supervisor in Beijing Normal University, for giving me the opportunity to take part in the joint program to study aboard and giving me a relaxing study environment. Thank you for training me with basic scientific thoughts and build a solid foundation of scientific research. Moreover, thank you for keeping excellent communication about the topic of my thesis and your understanding did me a good favour that makes it possible for me to finish this research.

My sincere thanks to my advisor Dr. Yinwen Sun, who helped me a lot with many obstacles to ensure the research can finish on time. Also, thanks to Dr. Yousif Hussin and assessment board during my proposal, for the constructive comments and suggestion for completion of this thesis. Moreover, I would like to thank ITC staff, especially my course director Dr. R.G. Nijmeijer, who helped me with the difficulties during the study in ITC; and all the teachers who taught in different courses, let me learn a lot of knowledge on remote sensing, geo-information and natural resource management.

My gratitude and appreciation for all my classmates and Chinses friends in ITC. Thanks for your company, help and coordination during every discussion, group work, field work and even parties. Thanks for encouraging me to be better and brave when facing the bright future.

Finally, my sincerest thanks to my parents for unconditional physical and spiritual support during the MSc life in ITC.

TABLE OF CONTENTS

LIST OF FIGURES

LIST OF TABLES

1. INTRODUCTION

1.1. Background

The intertidal zones are commonly regarded as one of the most valuable and active wetland ecosystems, due to its biological productivity (Lobato et al., 2016; Swennen et al., 1982; Zhang et al., 2016), economic value (Han & Yu, 2016), and ecological functions (Costanza et al., 1998). The intertidal zones represent the areas which are above water at low tide and under water at high tide, occupying the upper edge of the global coastlines extending more than 1.6×10^6 kilometres (Ortega-Morales et al., 2010). Generally composed of rocky platforms, sandy beaches, mud flats, estuaries and salt marshes (Bertness et al., 2001), the intertidal zones provide essential habitats for a wide range of both marine (Yates et al., 2014) and terrestrial (Rog et al., 2017) life. Due to daily tidal cycles, the intertidal zones are characterized as highly dynamic environments, which cause variations of moisture, temperature, nutrients and soil salinity (Menge & Branch, 2001). These environmental limitations influence marine and terrestrial biodiversity through food chains and interactions, resulting in different evolutions from the same microorganisms or microbial groups in order to be better adapted to these extreme environments (Ortega-Morales et al., 2010).

However, such valuable wetland ecosystems are facing a huge threat. Increasing anthropogenic pressure, climate change and sea level rise affect intertidal ecosystems (Giri et al., 2011) and decrease the area (Han & Yu, 2016; Ottinger et al., 2013) of them. Plant communities in the intertidal zones are also disappearing and degenerating, which is not only caused directly by land reclamation, land transformation, overexploitation and pollution, but also indirectly by trophic downgrading (Estes et al., 2011) and climate change (Jackson et al., 2001; Waycott et al., 2009). In China, the intertidal zones of the Yellow River Delta encountered adverse degradation and disappearance (Sun et al., 2017) by tidal flat reclamation (Ma et al., 2015) and hydrological condition deterioration (Zhang & Li, 2006). The lost area of tidal flats in the Yellow River Delta was 15699 hm^2 from 2001 to 2008, which is equal to 68.8 million Yuan per year in ecological compensation according to the market value and 103.6 million Yuan per year based on ecosystem services value (Han & Yu, 2016). Moreover, the area of shrubland in the Dongying Municipality, which is located in the main Yellow River basin, reduced by 811.7 km^2 from 1995 to 2010 (Ottinger et al., 2013). Therefore, this severely damaged intertidal ecosystem within the Yellow River Delta, which was designated as globally crucial under the Convention on Wetlands in the year of 2013 (Ramsar, 2013), is becoming a focus of the wetland conservation and research.

Plant communities are the key components of intertidal ecosystems (Kokaly et al., 2003; Yuan & Zhang, 2006) and indicate the health of the ecosystem, providing early signs of ecological degradation (Dennison et al., 1993; Silva et al., 2008). Plant communities in wetlands, having a capacity to remove toxic substance and heavy metals (Onaindia et al., 1996), are regarded as an indicator of water pollutions. Intertidal plant communities, such as Chinese tamarisk *(Tamarix Chinensis)*, which are highly sensitive to the variation of soil conditions (Liu et al., 2017), link a tight connection with the flooding pattern of the landscape of seasonal intertidal ecosystems. Moreover, intertidal plant communities provide habitats for wading birds and migratory birds (Ambrose, 1986), as well as prevent coastlines from soil erosion, playing a crucial role in shore protection and sediment retention (Costanza et al., 1998). Therefore, mapping the spatial distribution of intertidal plant communities is the primary step for degradation monitoring of intertidal ecosystem, because the change of vegetation distribution and succession reflects the change of soil condition and water content. In other words, for formulating tentative vegetation protection program, it is necessary to obtain updated spatial information on vegetation cover and distribution in the study area (He et al., 2005).

Figure 1 The landscape of the intertidal zones in the Yellow River Delta (photographed by Yansha Luo)

Traditional methods for mapping plant communities in the wetland are commonly hindered by limited data accessibility and time-consuming field work (Lee & Lunetta, 1995; Vis et al., 2003). Due to the unstable terrain and relatively tall plant species, wetlands usually have poor accessibility, and field work aiming at inventorying vegetation is usually expensive, time-consuming, and sometimes inaccurate (Lee, 1991). Satellite remote sensing technique has been widely used due to frequent acquisition, repeat coverage and low image cost (Hardisky et al., 1986; Klemas, 2001; Ozesmi & Bauer, 2002; Silva et al., 2008), provides efficient and economical approaches to classify plant communities and estimates related biophysical and ecological parameters (Adam et al., 2010). The application of satellite images makes it possible for a comprehensive understanding of the research objects and the changes in the past years (Bhandari et al., 2012; Vrieling et al., 2017).

The information on surface reflectance and emissivity characteristics can be obtained from optical images, of which the application for mapping plant communities has been studied for a long time, and many classification techniques have been proposed in the literature. Gómez et al. (2016) presented a range of data availabilities for optical image sources and various classification methods for plant communities. Ozesmi and Bauer (2002) summarised the application of satellite remote sensing for studying wetlands, with an emphasis on the various classification techniques used for wetlands identification. The mission of Sentinel-2 provides information for agriculture and forestry practices, aiming at mapping changes in land cover and monitoring the world's forests (Sentinel Hub, 2016). The use of Sentinel-2 data has been assessed successfully for crop and tree species classification (Immitzer et al., 2016) due to its higher spatiotemporal resolution than Landsat and SPOT, and three red edge bands which are of high sensitivity to the chlorophyll in vegetation. Csillik & Belgiu (2017) reported the results of dedication to cropland mapping from multi-temporal Sentinel-2 data using objects as spatial analysis units. Moreover, Traganos & Reinartz (2017) addressed the suitability of the Sentinel-2 satellite for mapping the distribution of Mediterranean seagrass meadows, which shows advantages for mapping wetland plant communities.

Recent years, remote sensing images utilized for land cover classification (Rogan, 2004) are increasingly from optical satellites to synthetic aperture radar (SAR) sensors, which can capture the dielectric properties and the structural features of the Earth surface objects. High-resolution, day-and-night and cloud-independent SAR data with different wavelength and polarization modes are being focused on the spectral and polarimetric dimensions. They are increasingly explored (Martinez & Letoan, 2007; Sartori et al., 2011) because of the sensitivity to plant moisture, canopy texture and surface roughness (Hess et al., 1995; Hess et al., 1990), all of which are regarded as essential characteristics for distinguishing wetland types (Baghdadi et al., 2004). The texture derived from SAR images are more attractive considering the inherent speckle noise that makes the single pixel confusing. Due to the microwave penetration within the canopies of vegetation, SAR images are sensitive to the underlying water in vegetation canopies (Martinez & Letoan, 2007). Also, Benefit from the C-band, Sentinel-1 data have a capacity for penetrating and receiving the backscattered signal, which provides detailed information on vegetation canopies and ground surface (Fu et al., 2017). The relatively high spatiotemporal resolution make it advantageous in discriminating rice agriculture and crop (Kumar et al., 2017; Torbick et al., 2017). Fu et al. (2017) successfully evaluated the performance of random forest algorithms for mapping wetland plant communities using L-band PALSAR and C-band Radarsar-2 data. Furtado et al. (2016) demonstrated that "single-season full-polarimetric C-band data could yield more accurate classifications than single-season dual-pol C-band SAR imagery and similar accuracies to dual-season dual-pol C-band SAR classification". Vegetation types with dense canopies were accurately classified using dual-season full-polarimetric SAR data and achieved high producer's and user's accuracies. Horritt et al. (2003) used SAR images of a salt marsh to investigate the radar backscattering properties of emergent marsh plant species and successfully map the inundated vegetation with a statistical active contour model. Simard et al., (2000) found texture measures from Japanese Earth Resources Satellite-1 are essential characteristics for the distinguishing submerged vegetation in Central Africa.

Considering seasonal variations in the spectral features and separability of image spectra, increasing vegetation classifications have relied on seasonal changes and phenological attributes through multi-season or multi-temporal images instead of a single-date image. Multi-season or multi-temporal images which capture spectral differences based on vegetation phenology, especially the spectral reflectances at peak biomass (Schmidt & Skidmore, 2003; Spanglet et al., 1998), help to improve separability of vegetation types over classifications compared with using a single-date image (DeFries et al., 1995). The high discrimination potential and capabilities in vegetation mapping applications have been shown through exploiting multi-temporal satellite images (Belluco et al., 2006; Dennison & Roberts, 2003; Judd et al., 2007), e.g. for assessing wetland vegetation in regularly flooded landscapes (Wang et al.,2012). Guerschman et al. (2003) explored how many dates of Landsat TM images needed to perform better to obtain an accurate land cover map in the Argentine Pampas. Gilmore et al. (2008) examined the effectiveness of using multi-temporal multispectral images for classifying and mapping the common plant communities of the Ragged Rock Creek marsh. Villa et al. (2012) demonstrated the capabilities of multi-sensor multi-temporal remote sensing in analyzing the spatial patterns and temporal trajectories of vegetation damage and recovery. Villa et al. (2015) showed the capabilities of multi-temporal reflectance and vegetation indices in mapping four macrophyte community types. Additionally, multi-temporal SAR images have also proven to be useful in urban, forest, and agriculture land cover classification (Le Toan et al., 1989; Pellizzeri et al., 2003; Quegan et al., 2000).

Normalized Difference Vegetation Index (NDVI) is a common and widely used vegetation index for vegetation monitoring (Nageswara et al., 2005; Tucker, 1979). It is applied in research on crop cover (Ayyangar et al., 1980), drought monitoring (Singh et al., 2003) and agriculture drought assessment for detecting global environmental and climatic change (Bhandari et al., 2012). Time series NDVI data are used interatively to explore the main determinants of seasonality for the subsequent determination and classification of vegetation types (Halabuk & Mojses, 2015). Defries & Townshend (1994) used the monthly NDVI values in a global-extent land cover mapping with AVHRR data. Tang et al. (2017) investigated the spatiotemporal changes of vegetation growth in upper Shiyang river basin with their response to climate changes by using NDVI statistic. Pang et al. (2017) successfully combined NDVI with climate data to examine spatial and temporal variations in vegetation and the relationships between climate and vegetation for both the growing period and seasons during the period from 1982 to 2012 on the Tibetan Plateau. Li et al. (2017) analyzed the temporal changes in vegetation coverage using NDVI over

1982 – 2015, and combined topographical factors to interpret the spatial patterns of vegetation as well as quantified the contributions of anthropogenic factors to vegetation variations. Gandhi et al. (2015) validated the capability of NDVI derived from Landsat TM images for vegetation classification and change detection, and the results showed the NDVI was highly useful in detecting the surface features, which provides a possibility for distinguishing and mapping different vegetation through phenology difference.

1.2. Problem statement

The intertidal zones of the Yellow River Delta are one of the most important ecosystems in China due to its ecological functions and high economical productivity. However, over the past decades, deteriorating hydrological conditions (Zhang & Li, 2006) and intensive anthropogenic activities (Ma et al., 2015) disturbed this vulnerable ecosystem, resulting in an enormous loss of wetland resource (Han & Yu, 2016). Therefore, it is important to provide real-time monitoring of these intertidal zones. Mapping plant communities can be an effective way to reflect the real-time conditions of intertidal zones because these plant communities are regarded as the indicators of eutrophication and soil contamination (Dennison et al., 1993; Silva et al., 2008). However, few studies on mapping vegetation in this special and important landscape have been done. The reasons may lie in the poor data accessibility and the properties of intertidal zones. Firstly, since the intertidal zones are long and narrow areas along the coastlines, the spatial resolution of traditional satellite remote sensing is relatively coarse for detecting and monitoring. Secondly, since the intertidal zones are highly dynamic, and the ground surface is successively submerged and emerged due to the daily tides, higher temporal resolution data are necessary for higher mapping accuracy. Thirdly, the importance of intertidal zones may not be widely realized. To sum up, the lack of high-quality images and inadequate concern may lead to the research gap on mapping intertidal plant communities in the Yellow River Delta.

Optical remote sensing classification technique for vegetation mapping has been widely applied (Gómez et al., 2016). The Sentinel-2 image has great potential for mapping intertidal plant communities thanks to its improved spatial and temporal resolution as well as three red edge bands that are sensitive to chlorophyll content. Multi-temporal data may capture the seasonality or phenological variation in vegetation types through the spectrum which varies with the amount and percentage of plant pigments, leaf water content and leaf structure (Key, 2001; Reed et al., 1994) and therefore improve the accuracy of distinguishing different vegetation types. In some case, it is difficult to separate the plant communities in wetland ecosystems through single-date optical image, because most wetland vegetation species have the same basic components contributing to spectral reflectance, such as chlorophyll, carotene and other light-absorbing pigments (Kokaly et al., 2003; Price, 1992) at common growth season. Also, the mingle poses an obstacle to distinguish plant communities (Guyot, 1990; Malthus & George, 1997). However, cases were also found that single-date image classification resulted in higher accuracy in some landscapes (Key, 2001). Therefore, it is worth exploring the capability of single-date image and comparison with multi-temporal images for classification and mapping the plant communities in such a dynamic and extreme ecosystem.

The combination of SAR and optical data is proposed to monitor wetland (Adam et al., 2010; Fu et al., 2017; Ozesmi & Bauer, 2002), and many studies have been carried out on the mapping wetland vegetation (Demers et al., 2015; Fu et al., 2017). Optical images contain the information on surface reflectance and emissivity characteristics, while SAR images capture the dielectric properties and the structural features of the Earth surface objects. The complementary information contained in the two sensors always significantly improve mapping accuracies based on using an individual sensor for certain land cover types, such as agriculture (Blaes et al., 1969; Chust et al., 2004) and wetlands (Augusteijn & Warrender, 1998a; Li & Chen, 2005). However, it is rare to find researches on mapping intertidal plant communities through the combination of Sentinel-1 SAR and Sentinel-2 optical images, not to mention using multi-temporal time series data. This research gap may be caused by poor data availability and high cost for good-quality images. Since the advent of Sentinel-1 and Sentinel-2 satellites, which are regarded as the free sources of high-quality image data, made it possible for catching the characteristics of plant communities in such a fluctuant environment. Therefore, it is worth exploring the integrated use of Sentinel-1 and Sentinel-2 time series data to map plant communities in the intertidal zones of the Yellow River Delta.

1.3. Research objective

The overall objective of this study is to map plant communities in the intertidal zones of the Yellow River Delta using Sentinel-1 SAR and Sentinel-2 optical data. The specific objectives of this research are to map intertidal plant communities in the Yellow River Delta using:

1) Single-date Sentinel-2 images for four different seasons (i.e., spring, summer, autumn and winter).
2) Multi-season (the aggregation of the four single seasons into a single dataset) Sentinel-2 images.
3) Time series (the aggregation of twelve monthly time series data into a single dataset) Sentinel-2 images.
4) NDVI statistic parameters derived from time series Sentinel-2 images.
5) Time series Sentinel-2 images and the NDVI statistic parameters derived from time series Sentinel-2 images.
6) Time series Sentinel-1 VV and VH data.
7) Time series Sentinel-2 images, NDVI statistic parameters, and time series Sentinel-1 VV and VH data.

1.4. Research questions

1) Is there a significant difference in intertidal plant communities mapping accuracies between the use of four single-date Sentinel-2 images? How does the accuracies of intertidal plant community classification vary with the four single-season images?
2) Does multi-season Sentinel-2 images significantly improve the classification of the intertidal plant communities compared to a single season?
3) Is there a significant difference in intertidal plant communities mapping accuracies between the use of multi-season and time series Sentinel-2 images?
4) What is the intertidal plant communities mapping accuracy derived from the NDVI statistic parameters?
5) Does adding NDVI statistic parameters to the time series Sentinel-2 images further improve the intertidal plant communities mapping accuracy?
6) What is the intertidal plant communities mapping accuracy derived from time series Sentinel-1 VV and VH data?
7) Does adding Sentinel-1 time series data to the time series Sentinel-2 images and NDVI statistic parameters can significantly improve the intertidal plant communities mapping accuracy?
8) Which input variables of satellite images contribute most to the accuracy of intertidal plant communities mapping?

1.5. Hypotheses

1) Hypothesis 1

H_0: There is no statistically significant difference in intertidal plant communities mapping accuracies between the use of four single-date and multi-season Sentinel-2 images.

H_1: The intertidal plant communities mapping accuracy derived from multi-season Sentinel-2 images is statistically significantly higher than the one derived from four single-date images.

2) Hypothesis 2

H_0: There is no statistically significant difference in intertidal plant communities mapping accuracies between the use of multi-season and time series Sentinel-2 images.

H_1: The intertidal plant communities mapping accuracy derived from time series Sentinel-2 images is statistically significantly higher than the one derived from multi-season Sentinel-2 images.

3) Hypothesis 3

H_0: There is no statistically significant difference in intertidal plant communities mapping accuracies between the use of time series Sentinel-2 data with and without NDVI statistic parameters.

H_1: Adding NDVI statistic parameters can significantly improve the intertidal plant communities mapping accuracy.

4) Hypothesis 4

H_0: There is no statistically significant difference in intertidal plant communities mapping accuracies between the use of the single sensor (Sentinel-1 or Sentinel-2) time series data and the combination of them.

H_1: The combination of Sentinel-1 and Sentinel-2 time series data can significantly improve the mapping accuracy of the intertidal plant communities based on using the single sensor time series data.

2. MATERIALS AND METHODS

2.1. Study area

The study area is in the intertidal zones of the Yellow River estuary (37°32'N - 37°54'N, 118°39'E – 119°21'E), which is part of the Yellow River Delta National Reserve situated in the northeast of Dongying City, Shandong Province, China. The modern Yellow River Delta shifted the mouth of the Yellow River to the north in the year of 1855, which is flanked to the west of the Laizhou Bay and the south of the Bohai Bay (Zhao et al., 2016).

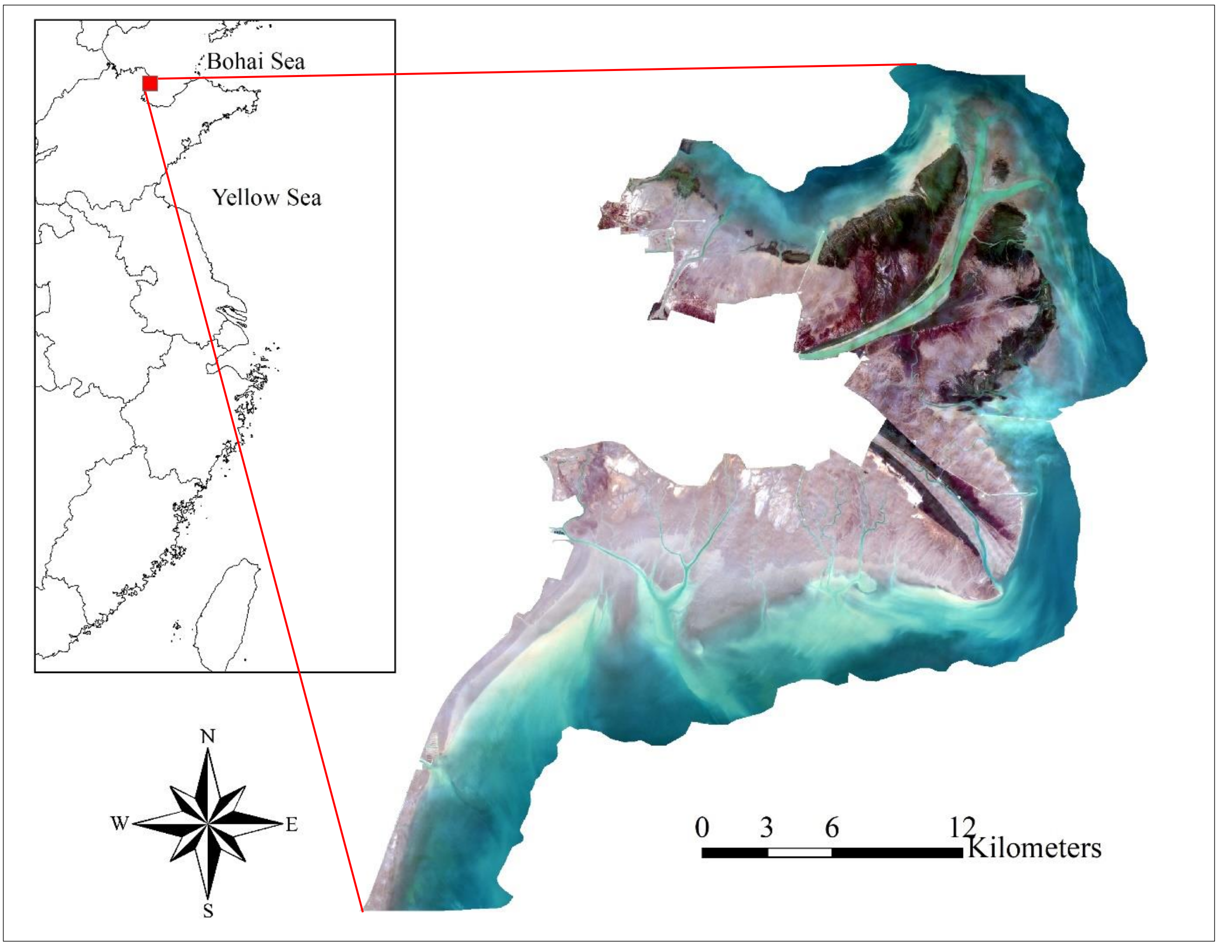

Figure 2 The location of the study area in the Yellow River Delta (display in RGB band 4,3,2)

The study area covered by the delta plain is 7879 kilometres with about 15 meters average deposition thickness (Wang et al., 2010). The tides in this intertidal zone are irregular semidiurnal tides with 0.73-1.77 meters of the mean tidal range (Li et al., 1991), which play an important role in hydrodynamics and controlling sedimentation in intertidal zones (Sun et al., 2015). Figure 3 shows the average monthly temperature and rainfall for Dongying City from the year of 1971 to 2000, which reflects that this nature reserve is of typical temperate monsoon climate, with an average annual temperature of 12.1℃, an average annual evaporation of 1962 mm and average annual precipitation of 551.6 mm (Sun et al., 2017), resulting in a typical water limitation that water resources are only river discharge and groundwater extraction (Kong et al., 2015).

The Yellow River Delta supports abundant biodiversity and provides large extend habitat for 220 seed plant species, 800 wild animal species and 283 bird species, many of which are in the list of endangered species (Cui et al., 2009). The Yellow River Delta is covered by wetlands with an area of 4167 km^2, consisting of 3131 km^2 of natural wetlands (marshes, mud flats, swamps, open water, etc.) and 1036 km^2 of artificial wetlands (aquaculture ponds, rice field, channels, etc.) (Qi & Fang, 2009). The dominant marsh type is coastal marsh, covering 63.03% of the entire Yellow River Delta (Cui et al., 2009), with four dominant vegetation species: Smooth cordgrass *(Spartina alterniflora)*; Seepweed *(Suaeda salsa)*; Common reed *(Phragmites australis)*; Five-stamen tamarisk *(Tamarix chinensis)*. The sequence of geomorphic units consists of high marsh, middle marsh and low marsh (Song et al., 2010). The high marsh zone is dominantly covered by Smooth cordgrass and Five-stamen tamarisk, while the middle and low march zones contain large bare soil interspersed with patches of Smooth cordgrass. And Common reed appears at the terrestrial boundary of the marsh (Li et al., 2016). However, the reed marsh, meadow and tidal wetland decreased by 17%, 37% and 38% respectively from the year 1986 to 2001 caused by decreased runoff and conversion to aqua-cultural ponds and agricultural fields (Li et al., 2009).

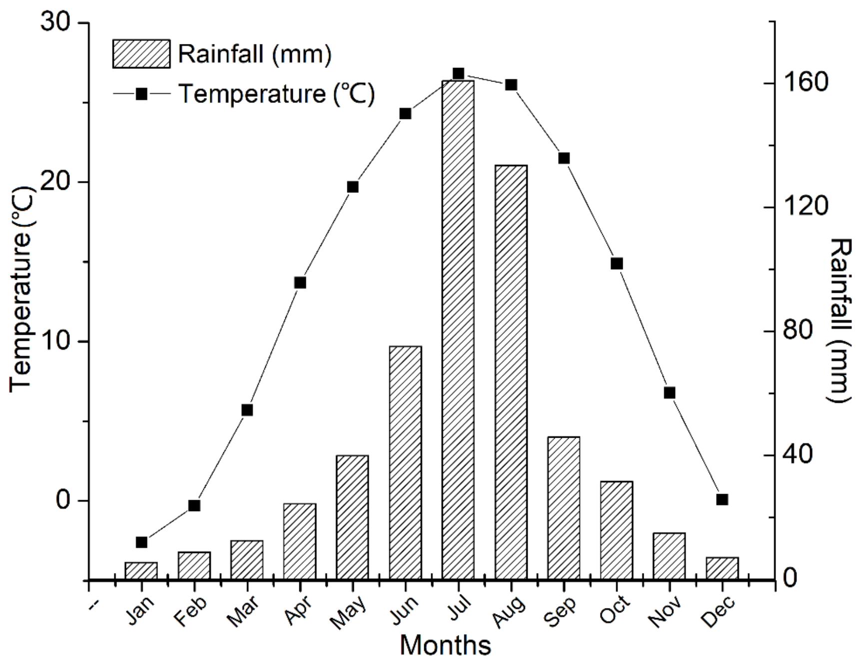

Figure 3 The average monthly temperature and rainfall for Dongying City from the year of 1971 to 2000

2.2. Data preparing and processing

2.2.1. Sentinel-2 data and Pre-processing

Sentinel-2 consists of two optical satellites (i.e., Sentinel-2A and Sentinel-2B), which were launched in June 2015 and March 2017 respectively (Suhet, 2015). Sentinel-2 serves a wide range of applications including various plant indices determination, effective yield prediction, and providing information for agriculture and forestry practices which related to Earth's vegetation. Especially, Sentinel-2 can be used for mapping changes in land cover and to monitor the forests in global scale (Sinergise, 2017).
They are commonly used in:

- Environmental monitoring through monitoring land cover and land use change
- Agricultural applications, such as crop monitoring for helping food security management
- Detailed vegetation and forest monitoring and parameter generation (e.g. leaf area index, chlorophyll concentration, carbon mass estimations)
- Coastal zones observation (marine environment monitoring, coastal zone mapping)
- Inland water (lake, river, reservoir) monitoring
- Glacier monitoring, ice extent change, snow cover monitoring
- Flood mapping and management (risk analysis, loss assessment, disaster management during floods)

The spectral and spatial resolution characteristics of Sentinel-2 images are shown in Table 1. In this study, twelve multi-temporal Sentinel-2 images with band 2~7, 8a, 11 and 12 from July 2016 to July 2017 are acquired from the Copernicus Open Access Hub (https://scihub.copernicus.eu/dhus/#/home) of European Space Agency (ESA) and these images were atmospherically corrected in the software Sen2cor module version 2.2.1 within the Sentinel-2 Toolbox (S2TBX) and all images were resampled to 20 m. The used Sentinel-2 optical time series data are shown in Figure 4.

Table 1 Overview of the Sentinel-2 data

Band	Wavelength range (nm)	Spatial resolution (m)	Purpose
Band 1- Coastal aerosol	433 - 453	60	Aerosol detection
Band 2 - Blue	458 - 523	10	Soil and vegetation discrimination, forest type mapping, man-made features
Band 3 - Green	543 - 578	10	Clear and turbid water, vegetation
Band 4 - Red	650 - 680	10	Identifying vegetation types, soils and urban features.
Band 5 - Red edge	698 - 713	20	Classifying vegetations
Band 6 - Red edge	733 - 748	20	Classifying vegetations
Band 7 - Red edge	773 - 793	20	Classifying vegetations
Band 8 - Near infrared	785 - 900	10	Classifying vegetations
Band 8A - Near infrared	855 - 875	20	Mapping shorelines and biomass content, detecting and analysing vegetation
Band 9 - Water vapour	935 - 955	60	Detecting the water vapour
Band 10 - Shortwave infrared / Cirrus	1360 - 1390	60	Cirrus cloud detection
Band 11 - Shortwave infrared	1565 - 1655	20	Moisture content of soil and vegetation, snow and clouds
Band 12 - Shortwave infrared	2100 - 2280	20	Snow/ice/cloud discrimination

Figure 4 Time series Sentinel-2 data used in the study (display in RGB band 4,3,2)

To improve the accuracy of intertidal plant community mapping, the vegetation index NDVI705 was selected as an additional input variable. The vegetation index NDVI705 is a modification of the common used NDVI, from which it differs by using bands along the red edge bands with a very narrow bandwidth. And it takes advantage of the sensitivity of red edge bands to small changes in canopy foliage content, gap fraction and senescence (Sinergise, 2017). Four statistic parameters (i.e., maximum, minimum, mean and standard deviation) were calculated in ENVI as the input variables for image classification, shown in Figure 5. The calculation equation of DNVI705 is:

$$NDVI705 = \frac{B06 - B05}{B06 + B05}$$

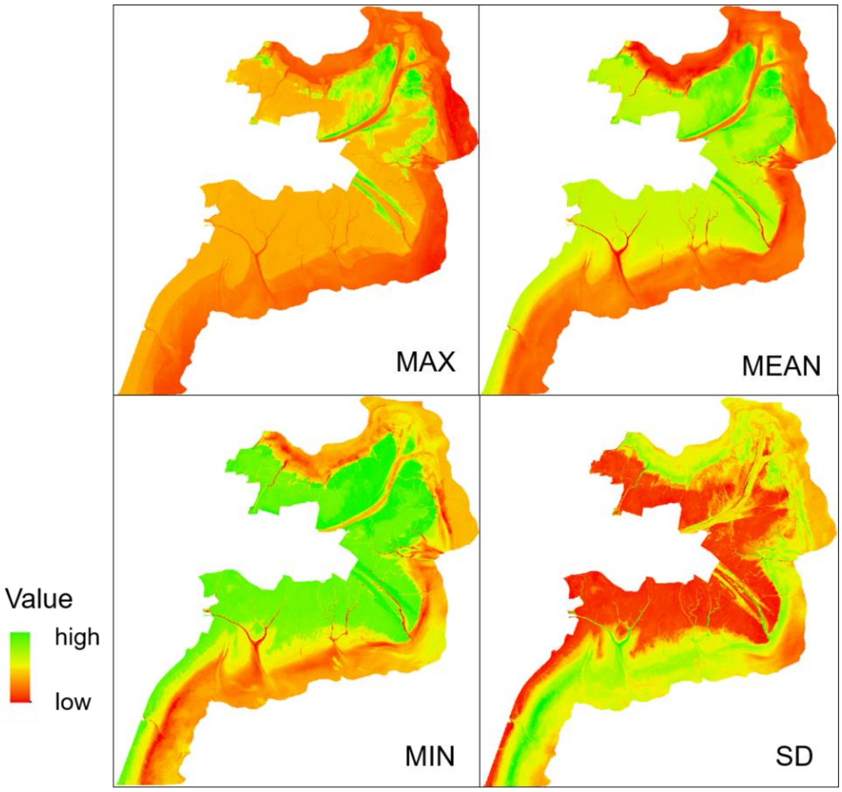

Figure 5 NDVI statistic parameters derived from Sentinel-2 time series data

2.2.2. Sentinel-1 data and Pre-processing

Sentinel-1 provided continuity of data with enhancement on revisit, coverage, timeliness and reliability of service (Torres et al., 2012). The products of Sentinel-1 are mainly used for:

- monitoring sea ice zones and the arctic environment, and surveillance of marine environment
- monitoring land surface motion risks
- mapping of land surface: forest, water and soil
- mapping in support of humanitarian aid in crisis situations

Level-1 GRD images of Sentinel-1 product with IW mode and dual polarizations VV and VH were used in the study. Twenty-four images from July 2016 to July 2017 were acquired from the Copernicus Open Access Hub (https://scihub.copernicus.eu/dhus/#/home) of European Space Agency (ESA). The main characteristics of the Sentinel-1 IW data are provided in Table 2 (Torres et al., 2012). The Sentinel-1 SAR time series images used in this study are shown in Figure 3 and Figure 4.

Several pre-processing steps were implemented in the Sentinel Toolbox (SNAP) developed by ESA. The images were transferred from DN values to sigma backscatter images expressed in dB scale. The specific pre-processing steps are shown as follows:

1) Radiometric correction. Radiometric errors always exist in the Level-1 primary products, by using the tool Radar – Radiometric - Calibrate in SNAP, radiometric correction were achieved and resulted in backscatter σ_0.
2) Speckle filtering. Speckle noise, which is caused by coherent processing of backscattered signals, usually makes it difficult for image interpretation. To reduce the influence of speckles, the tool Radar-Speckle – Filtering - Single Product Speckle Filtering in SNAP was used. Meanwhile, a 3×3 pixel window in Refined Lee method was chosen to apply due to the function of conserving the edges.

3) Geometric correction. Caused by the side-view characteristic, distortions (overlapping and shadow) may reduce the quality of SAR images. Range-Doppler method in the tool Radar – Geometric - Terrain Correction was chosen for image registration. Meanwhile, the image resolution was resampled to 20 m using nearest neighbourhood method and projected to the UTM coordinate system.

Then, these processed SAR images were converted to TIFF format for further processing in GIS and ENVI software.

Table 2 Overview of Sentinel-1 data

Parameter	Interferometric Wide swath mode (IW)
Incidence angle range	29.1° - 46.0°
Swath width	250 km
Sub-swaths	3
Polarization	Dual VV+VH
Azimuth resolution	20 m
Ground range resolution	5 m
Azimuth and range looks	Single
Maximum Noise Equivalent Sigma Zero (NESZ)	-22 dB
Radiometric stability	0.5 dB (3 σ)
Radiometric accuracy	1 dB (3 σ)
Phase error	5°
Pixel size	10 m

Figure 6 Time series Sentinel-1 images with VV polarization used in the study

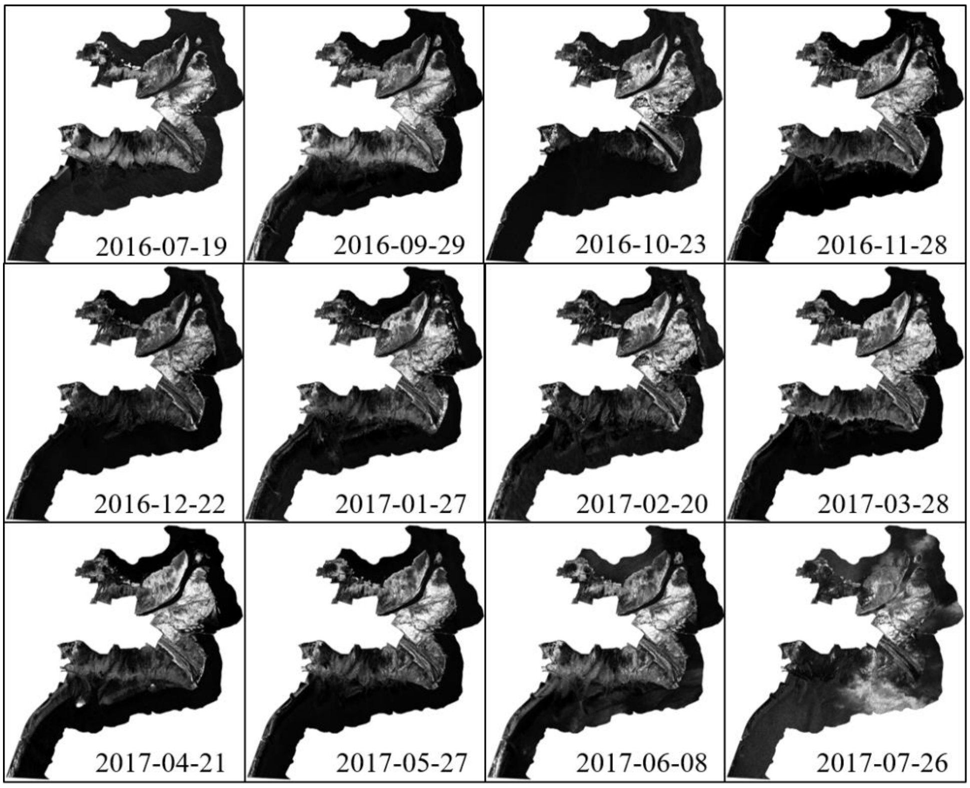

Figure 7 Time series Sentinel-1 images with VH polarization used in the study

2.2.3. Ground data collection

For the part of ground data collection, the pre-processing steps of selection classification criteria, development sampling strategy and selection sampling methods are the precondition for good field work. In this study, total vegetation cover from above (CFA), which means like a bird's eye view from above, within a delineated area on aerial image (Brohman et al., 2005) to estimate the relative percentages of non-overlapping vegetation cover, was selected as the attribute for structural classes determination. Vegetation classification criteria were determined based on the floristic composition. "Floristic classifications emphasize the plant species comprising the vegetation instead of life forms or structure and are based on community composition and diagnostic species" (Jennings et al., 2003). The community composition was based on the absolute amounts of each plant species present in a given area or stand, expressing the amount of each plant taxon as absolute percent cover. The diagnostic species are "any species or group of species whose relative constancy or abundance can be used to differentiate one vegetation type from another" (Jennings et al., 2003), which are determined empirically by analysis of filed work. "The dominance types are most simply defined by the single species with the greatest amount of canopy cover in the uppermost layer. Dominance types based on multiple species requires more rigorous data analysis and classification of dominance types requires canopy cover estimates for the species in the uppermost vegetation layer and the physiognomic attributes" (Jennings et al., 2003).

In this study, ground observation data for image classification and verification were collected in the field during October 2017. Stratified random sampling scheme was build and stratification of the study area was based on the landscape distribution map generated in the research of Wanlong Sun (Sun et al., 2017), combining with obvious physiognomic types in the field. Random sample plots were generated in ArcGIS while actual sample plots were adjusted according to the guidelines:

- The plot should include plant communities with homogeneous physiognomy

- The predominant type in the same vegetation layer should be consistent
- The plot should not encompass any abrupt changes or obvious gradients in environmental factors, such as slope, aspect, geologic parent materials etc.

A software named MAP PLUS uploaded in mobile phone was used for navigation with a 0.6-meter accuracy. Each sample point in the field represented approximately 30 * 30 m sample plot, and each plot was divided into five subplots oriented towards each cardinal direction and centre point as shown in Figure 9. The percentage of plant taxa in each subplot was documented and the sum was calculated for each sample plot. Based on vegetation cover, dominance types were identified and classified into seven classes of plant communities and two classes of non-vegetation landscapes as shown in Figure 8. The description of nine classes was shown in Table 3. In addition, UAV technique was used to provide reference information on class identification due to poor accessibility. Totally, 370 sample plots were identified and collected in study area with 30 – 50 samples for each stratum.

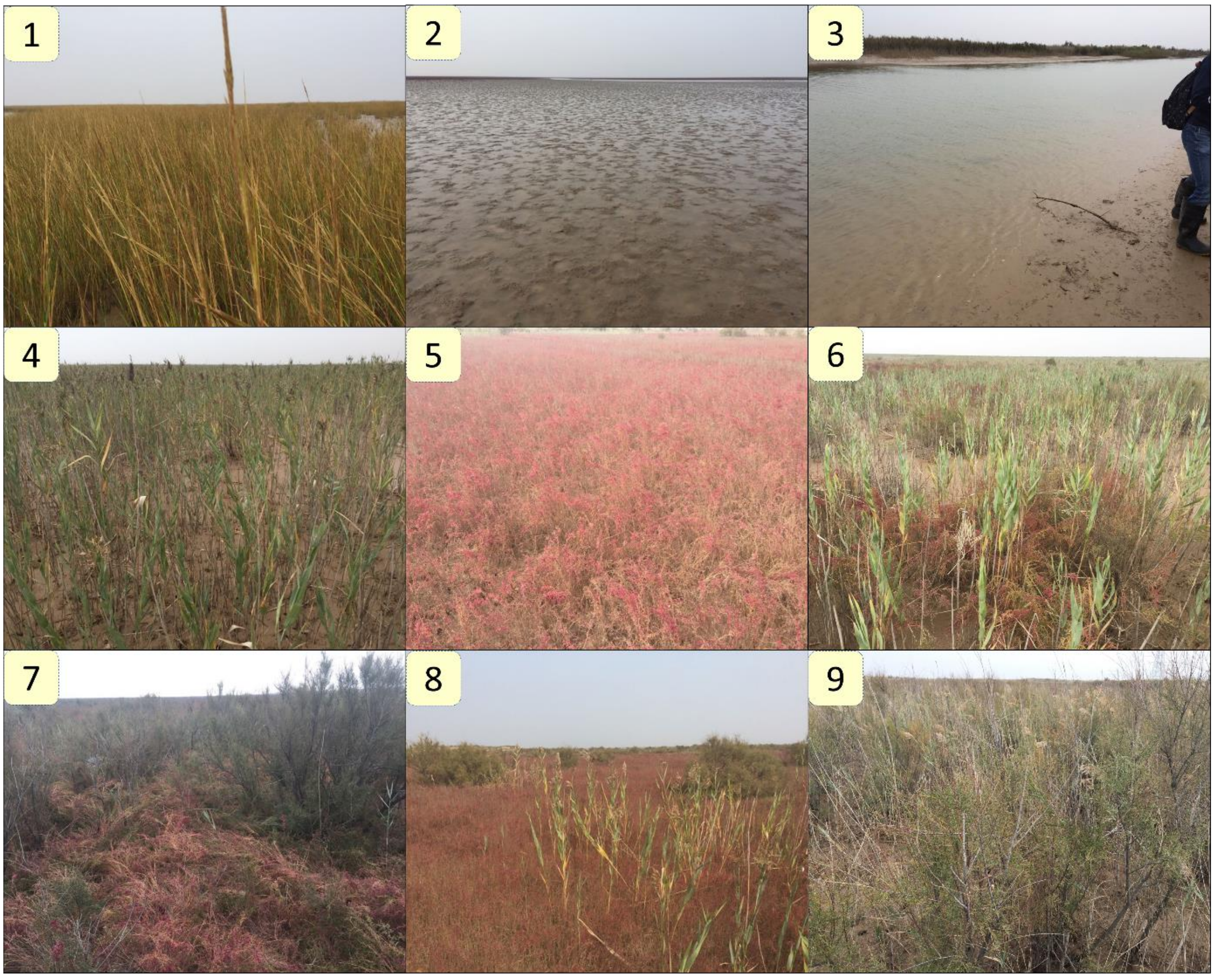

Figure 8 Field photos of the nine classes mapped. 1) Cordgrass; 2) Mud flats; 3) Open water; 4) Reed; 5) Seepweed; 6) Seepweed + Reed; 7) Seepweed + Tamarisk; 8) Seepweed + Tamarisk +Reed; 9) Tamarisk + Reed.

Table 3 Nine-categories plant communities and non-vegetation landscape description

Class	Description
1-Cordgrass	Smooth cordgrass has > 70%
2-Mud flats	Total vegetation plot cover < 5%
3-Open water	Includes transient water that obscures other classes and permanent water where the water table is above the ground channel, river and sea.
4-Reed	Common reed has > 70%
5-Seepweed	Seepweed has > 70%
6-Seepweed + Reed	Seepweed and Common reed in combination > 80%
7-Seepweed + Tamarisk	Seepweed and Five-stamen tamarisk in combination > 80%
8-Seepweed + Tamarisk + Reed	Seepweed, Common reed and Five-stamen tamarisk in combination > 80%, each vegetation type > 20%
9-Tamarisk + Reed	Five-stamen tamarisk and Common reed in combination > 80%

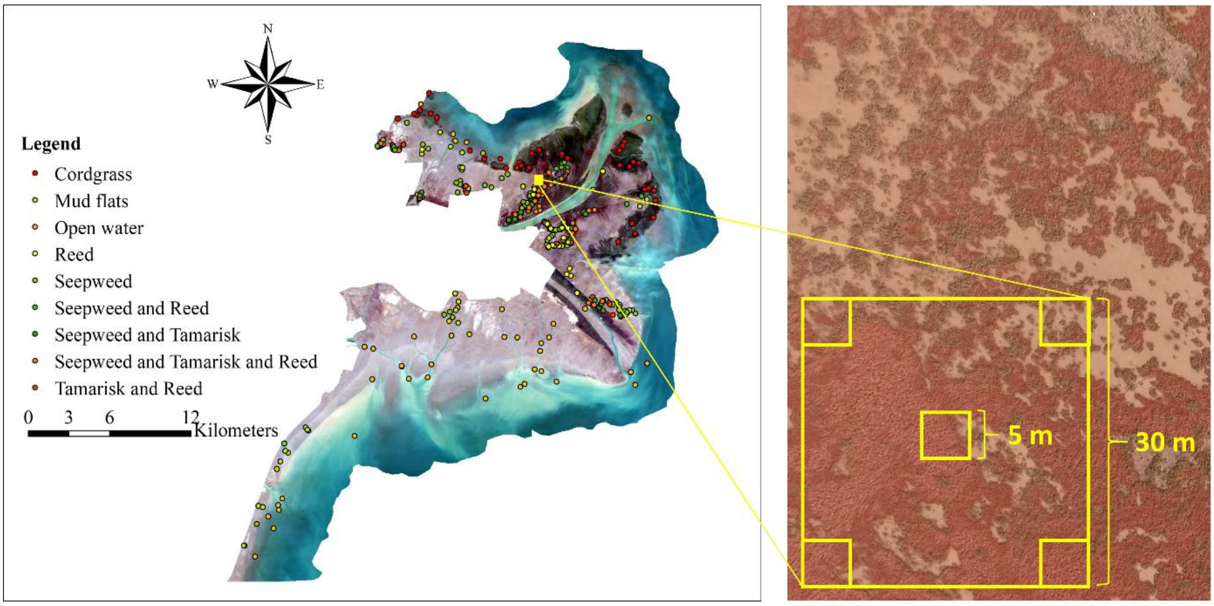

Figure 9 Distribution of sample plots in the study area and diagram of stratified sample method

2.3. Methods

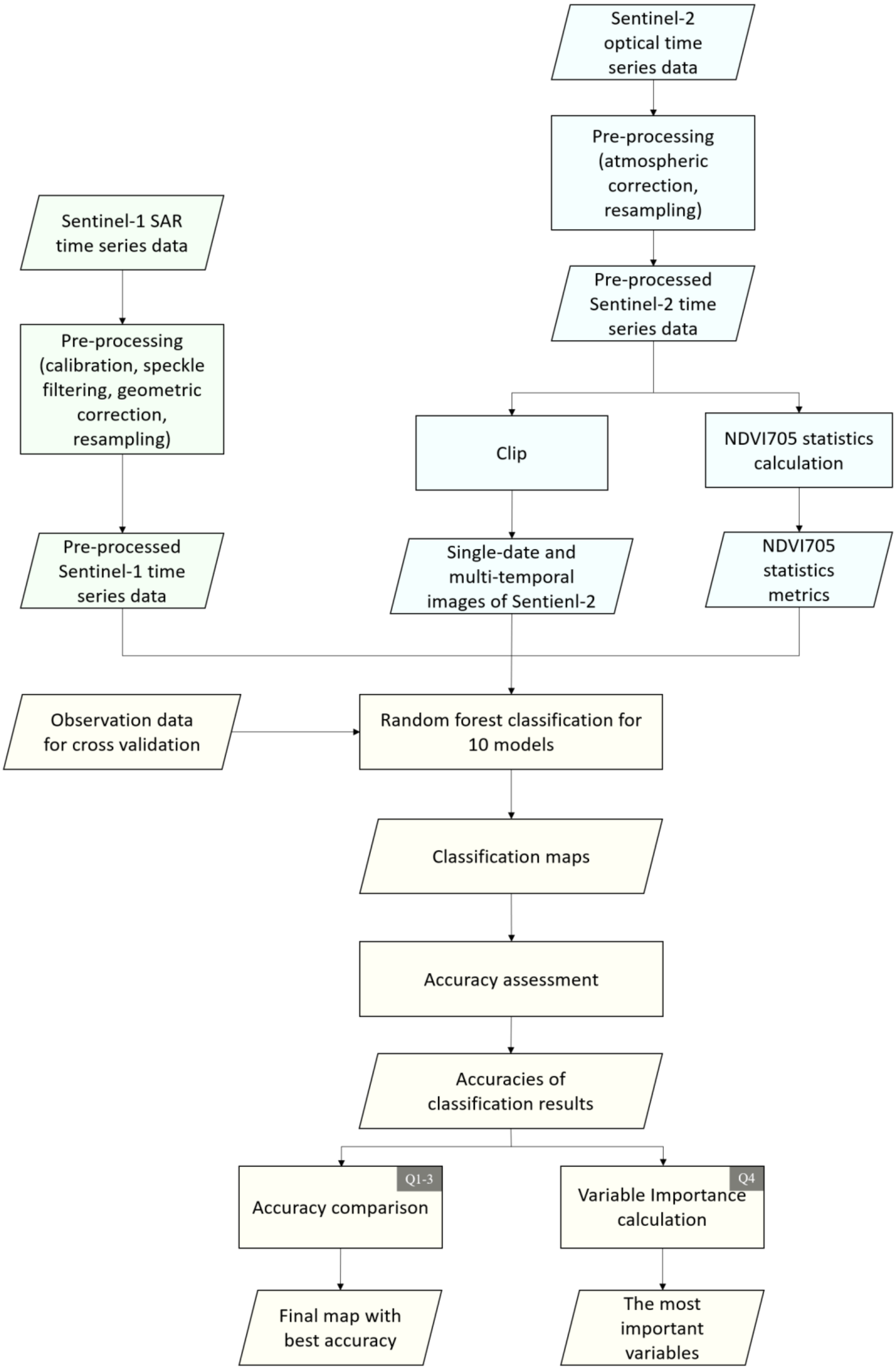

Figure 10 Flowchart of research methodology

2.3.1. Random Forest Algorithm

Random Forest (RF) classifier is widely used in various remote sensing classification (Lu & Weng, 2007). As one type of supervised classifiers based on machine learning, random forest classifier can easily detect the spectral characteristics of vegetation from ground training data and identify these unidentified data with the trained characteristics (Belgiu & Drăguţ, 2016). Compared with other machine learning classifiers, random forest classifier can usually get a higher accuracy of classification results (Abdel-Rahman et al., 2014; Shang & Chisholm, 2014). Also, the requirement for fewer parameters (Chan et al., 2012; Shao et al., 2015) and less time (Chan & Paelinckx, 2008a) make it advantageous over other classifiers, especially when using multi-dimensional data. Moreover, random forest classifier has been widely applicated to map land cover classes (Colditz & Roland, 2015; Haas & Ban, 2014), boreal forest habitats (Räsänen et al., 2013) and tree canopies (Karlson et al., 2015). Therefore, random forest classifier was used for classifying and mapping intertidal plant communities in this study.

Random Forest is a collective classifier combining a range of decision trees which make it advantageous for classification (Breiman, 2001). These trees are individually established by a bootstrapped sample of the training dataset (Pal, 2005). After several trees grow, the tree will be split using a user-defined number of input variables (i.e., Mtry) randomly selected at each node. When the established forest gets the user-defined number of trees (i.e., Ntree), each tree will vote for the best input variable using the bootstrapped samples. So the forest casts the votes and chooses the classification with the majority votes (Millard & Richardson, 2013). In each tree, around half of the total samples (i.e., in-bag samples) are used to train the trees while the rest (i.e., out-of-bag samples) is used in an internal cross-validation technique for estimating model accuracy. In other words, each tree is trained using a certain percentage of randomly selected training points with the remaining of training data, serving to estimate the classification accuracy. The out-of-bag (OOB) error is estimated based on the error classification, which the smaller indicates the higher accuracy of classification. Furthermore, the results derived from Random Forest Classification are not hindered by overfitting because a lot of trees generated ensures generalization of the patterns in the data (Breiman, 2001). In this classification, the value of 1000 for Ntree was proposed, and the Mtry value was the default.

Variable importance was evaluated by the difference in classification accuracies between the permuted and original out-of-bag samples (Breiman, 2001). To estimate the importance of input variable, the out-of-bag samples of the certain variable are randomly permuted first. The permuted out-of-bag samples are run through all the classification trees again. "Then the variable importance is computed by averaging the difference in accuracies between the original and the permuted out-of-bag samples for all the trees. The merit of the variable importance measure compared to univariate screening methods is not only includes the influence of each predictor variable separately but also the multivariable interactions with other predictor variables, which make this advanced approach more efficient and accurate" (Archer & Kimes, 2008; Chan & Paelinckx, 2008b). In this study, the Gini index was automatically derived from the random forest algorithm, indicating the importance of the input variables for all models with different combinations of satellite data.

2.3.2. Classification scenarios

In this study, random forest classifier was used to identify nine land cover classes (1-Cordgrass; 2-Mud flats; 3-Open water; 4-Reed; 5-Seepweed; 6-Seepweed + Reed; 7-Seepweed + Tamarisk; 8-Seepweed + Tamarisk + Reed; 9-Tamarisk + Reed) based on input variables derived from Sentinel-1 SAR and Sentinel-2 optical data in R platform. The input variables include Sentinel-1 SAR time series data with dual VV + VH polarization, single-date and multi-temporal Sentinel-2 images, NDVI statistic parameters (i.e., annual mean, maximum, minimum, and standard deviation) derived from time series Sentinel-2 data.

Ten scenarios which were combined with different input variables were implemented for plant community classification. For scenario 1 to scenario 4, four single-date images, captured on April 22 of 2017, July 11 of 2017, October 14 of 2016 and January 12 of 2017, were respectively selected as the representatives of the seasons of spring, summer, fall and winter. The selection of single-date images was according to the average monthly temperature and rainfall for Dongying City from the year of 1971 to 2000, which is shown in Figure 3. Scenario 5 combined multi-season (the aggregation of the four single seasons into a single dataset) Sentinel-2 images while scenario six combined total twelve multi-temporal Sentinel-2 images. Scenario 7 and scenario 8 explored the contribution of NDVI statistic parameters to intertidal plant communities mapping. Scenario 9 and scenario 10 explored the integration of Sentinel-1 SAR and Sentinel-2 optical time series data.

Table 4 Different scenarios of input variables for intertidal plant community classification

Scenarios	Input variables							Number of input variables
	Sentinel-2						Sentinel-1	
	Spring image	Summer image	Autumn image	Winter image	Time-series images	NDVI statistic parameters	Time-series VV and VH	
1	√							1
2		√						1
3			√					1
4				√				1
5	√	√	√	√				4
6					√			12
7						√		4
8					√	√		16
9							√	24
10					√	√	√	40

Note: Four Sentienl-2 images from different seasons were chosen as the single-date input data, which were captured from April 22th 2017 (spring), July 11th 2017 (summer), October 10th 2016 (autumn), January 12th 2017 (winter).

2.3.3. Accuracy Assessment

The performance of different classification results derived from ten ten-fold classification scenarios showing in different plant communities maps, were assessed in the confusion matrix, including overall accuracy, producer's accuracy, user's accuracy and kappa coefficient. The confusion matrix was widely used for accuracy assessment as a simple cross-tabulation for providing information of the predicted classes against the true field samples at the same certain locations (Foody, 2002). The overall accuracy was calculated from the total number of correctly classified samples divided by the total number of samples (Congalton, 1991). The producer's accuracy is the mapping accuracy from the point of view of the map producer, which reflects how often are the real feature on the ground correctly shown on the classification map; it equals to the number of reference sites classified accurately divided by the total number of reference sites for that class. User's accuracy is the accuracy from the point of view of a map user, which tells the users how often the class on the map will be present on the ground; it is calculated by taking the total number of correct classifications for a particular class and dividing it by the row total. The kappa coefficient is generated from a statistical test to evaluate the accuracy of classification, which evaluates how well the classification performed as compared to randomly assigning values; it represents the proportion of agreement obtained after removing the chance effect, which can range from -1 to 1. A value of 0 indicates that the classification is no better than a random classification while a negative number indicates the classification is significantly worse than random. A value closes to 1 indicates that the classification is significantly better than random.

In this study, the same sample sites for both classification and validating were used in accuracy assessment, which aims at guaranteeing the comparability between classification results. And ten-fold cross-validation analysis with the training dataset was performed. A total of 50% of the ground observation data were randomly selected in GIS for training the classifier, while the remaining 50% were used for mapping accuracy assessment. The confusion matrices, producer's accuracy, and user's accuracy were calculated using the remaining 50% for different scenarios. T-tests are wildly used in identification if the averages of two groups are statistically different. Two-sample t-tests were used for comparing two different samples. Furthermore, paired t-tests are used when observations from one group are paired with the other one. To test the significant difference between different scenarios, two sample paired t-test was proposed for the normally distributed population. In this study, the level of confidence is 95% ($\alpha = 0.05$). Thus, the result is considered to be statistically different when p-value < 0.05.

3. RESULTS

Due to the different combination of the input data, there are totally ten-fold classification results for each scenario, and for each part, the best classification result of each scenario was chosen to be shown.

3.1. Mapping intertidal plant communities using single−date Sentinel-2 image

Figure 11 – Figure 14 show the classification results of plant communities and non-vegetation classes in the intertidal zones of the Yellow River Delta respectively using four single-date images across seasons (i.e., spring, summer, autumn and winter). In these maps, obvious and distinctive differences in spatial distribution and extent of different types of plant communities were found, which reflected the large difference capability of single-date optical images when mapping intertidal plant communities.

The performances for intertidal plant community classification among various single-season images were observed; the season of autumn showed the overall accuracy of 63.58% ± 3.03% and the kappa coefficient of 0.59 ± 0.04, followed by the season of winter (overall accuracy 61.28% ± 2.03%, kappa coefficient 0.56 ± 0.02). And the seasons of spring (overall accuracy 57.36% ± 4.22%, kappa coefficient 0.52 ± 0.05) and summer (overall accuracy 58.51% ± 2.71%, kappa coefficient 0.53 ± 0.03) also showed lower capability for wetland vegetation classification.

For the best results among ten-fold classifications, the confusion matrix for the plant community classification derived from four single-season images is respectively presented in Table 5 – Table 8. According to Table 5, the classes of 6-Seepweed+Reed (producer’s accuracy = 21.43%, user’s accuracy = 37.5%) and 9-Tamarisk+Reed (producer’s accuracy = 30.77%, user’s accuracy = 40%) showed confusion classification to be other mixed classes which had the same vegetation species as themselves. In the confusion matrix of summer, around half of the class 4-Reed (producer’s accuracy = 34.78%, user’s accuracy = 57.14%) was misclassed to the other classed mixed with Reed, such as the classes of 6-Seepweed+Reed and 9-Tamarisk+Reed; more than half of the class 6-Seepweed+Reed (producer’s accuracy = 28.57%, user’s accuracy = 44.44%) were misclassified to 4-Reed and 7-Seepweed+Tamarisk. As for Table 7, the confusion matrix of autumn, the confusion classification mostly appeared in the classes of 2-Mud flats (producer’s accuracy = 60.00%, user’s accuracy = 50.00%) and 9-Tamarisk+Reed (producer’s accuracy = 53.85%, user’s accuracy = 63.64%). Most of the misclassification of 2-Mud flats wrong classified to 5-Seepweed while the some of the reference points of 9-Tamarisk+Reed were predicted to be 6-Seepweed+Reed. Finally, the Table 8 showed the classes of 2-Mud flats (producer’s accuracy = 40.00%, user’s accuracy = 44.44%), 4-Reed (producer’s accuracy = 50.00%, user’s accuracy = 46.67%) and 6-Seepweed+Reed (producer’s accuracy = 50.00%, user’s accuracy = 46.67%) were inclined to be respectively misclassified to 2-Mud flats, 6-Seepweed+Reed and 8-Seepweed+Tamarisk+Reed.

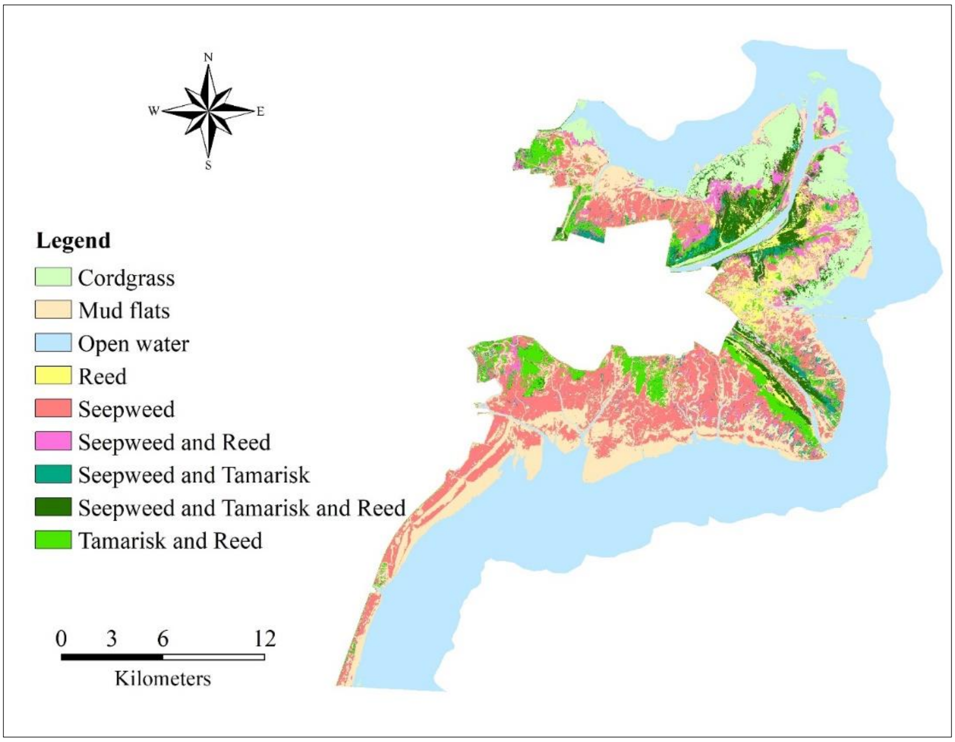

Figure 11 The map of intertidal plant communities produced using spring Sentinel-2 image

Table 5 Confusion matrix for nine-categories plant communities and non-vegetation landscapes classification derived from spring Sentinel-2 image

	Reference									User's
Prediction	1	2	3	4	5	6	7	8	9	accuracy （%）
1-Cordgrass	**13**	0	0	0	0	0	0	2	0	86.67
2-Mud flats	1	**14**	1	2	6	2	0	1	3	46.67
3-Open water	0	0	**17**	0	0	0	0	0	0	100.00
4-Reed	0	1	0	**8**	1	4	2	0	4	40.00
5-Seepweed	0	2	0	0	**9**	1	0	1	1	64.29
6-Seepweed+Reed	0	0	0	1	1	**3**	1	1	1	37.50
7-Seepweed+Tamarisk	1	1	0	0	0	1	**6**	2	0	54.55
8-Seepweed+Tamarisk+Reed	0	0	0	2	0	3	5	**13**	0	56.52
9-Tamarisk+Reed	0	2	0	1	1	0	2	0	**4**	40.00
Producer's accuracy （%）	86.67	70.00	94.44	57.14	50.00	21.43	37.50	65.00	30.77	
							Overall accuracy	58.78%		
							Kappa	0.60		

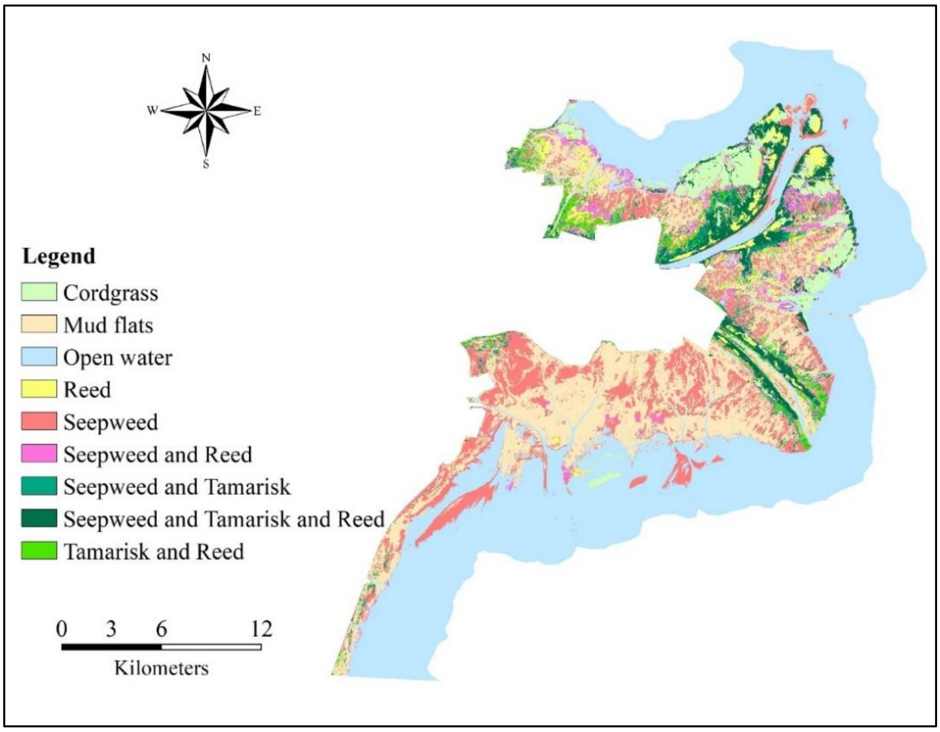

Figure 12 The map of intertidal plant communities produced using summer Sentinel-2 image

Table 6 Confusion matrix for nine-categories plant communities and non-vegetation landscapes classification derived from summer Sentinel-2 image

Prediction	Reference 1	2	3	4	5	6	7	8	9	User's accuracy （%）
1-Cordgrass	**13**	0	0	1	0	2	0	2	0	72.22
2-Mud flats	0	**13**	2	1	4	0	0	1	1	59.09
3-Open water	0	0	**14**	0	0	0	0	0	0	100.00
4-Reed	1	4	0	**8**	2	4	1	0	3	34.78
5-Seepweed	0	3	2	1	**10**	2	0	0	0	55.56
6-Seepweed+Reed	0	0	0	2	0	**4**	1	1	1	44.44
7-Seepweed+Tamarisk	0	0	0	0	0	2	**8**	3	0	61.54
8-Seepweed+Tamarisk+Reed	0	0	0	0	0	0	3	**12**	0	80.00
9-Tamarisk+Reed	1	0	0	1	2	0	3	1	**8**	50.00
Producer's accuracy （%）	86.67	65.00	77.78	57.14	55.56	28.57	50.00	60.00	61.54	
							Overall accuracy	60.81%		
							Kappa	0.57		

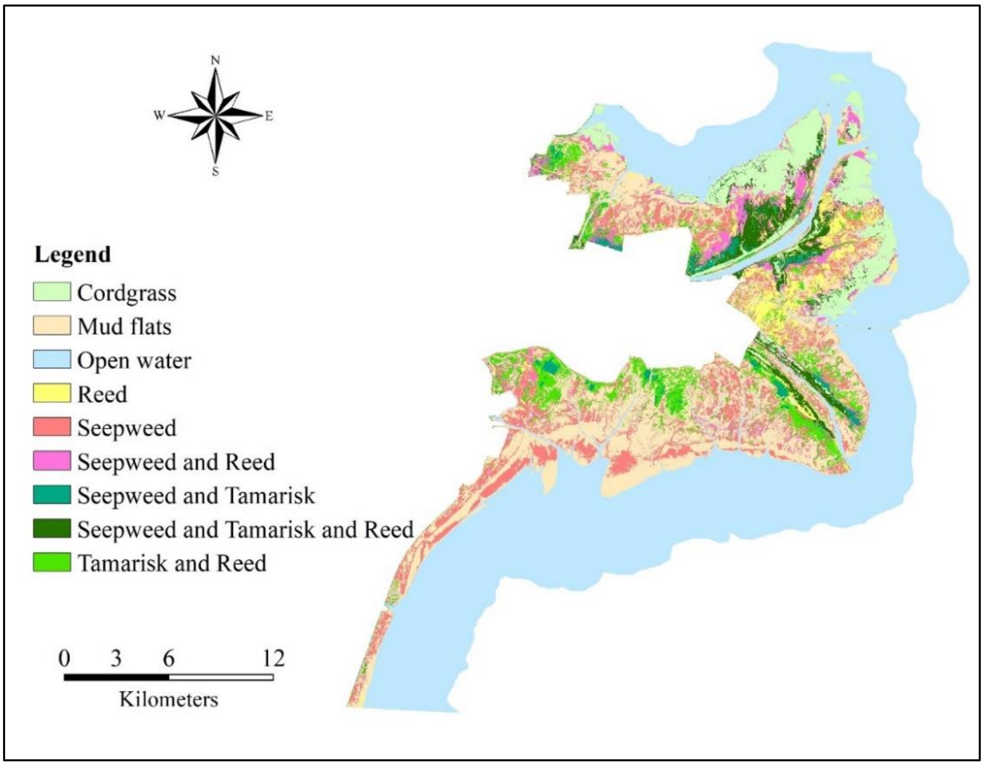

Figure 13 The map of intertidal plant communities produced using autumn Sentinel-2 image

Table 7 Confusion matrix for nine-categories plant communities and non-vegetation landscapes classification derived from autumn Sentinel-2 image

Prediction	Reference 1	2	3	4	5	6	7	8	9	User's accuracy （%）
1-Cordgrass	**13**	0	0	0	0	0	0	1	0	92.86
2-Mud flats	1	**12**	1	0	4	2	3	1	0	50.00
3-Open water	0	0	**17**	0	0	0	0	0	0	100.00
4-Reed	0	2	0	**12**	0	2	0	2	0	66.67
5-Seepweed	0	3	0	0	**11**	0	1	0	1	68.75
6-Seepweed+Reed	0	0	0	0	1	**10**	3	2	4	50.00
7-Seepweed+Tamarisk	1	0	0	0	0	0	**9**	2	1	69.23
8-Seepweed+Tamarisk+Reed	0	1	0	2	0	0	0	**12**	0	80.00
9-Tamarisk+Reed	0	2	0	0	2	0	0	0	**7**	63.64
Producer's accuracy （%）	86.67	60.00	94.44	85.71	61.11	71.43	56.25	60.00	53.85	
							Overall accuracy	69.59%		
							Kappa	0.66		

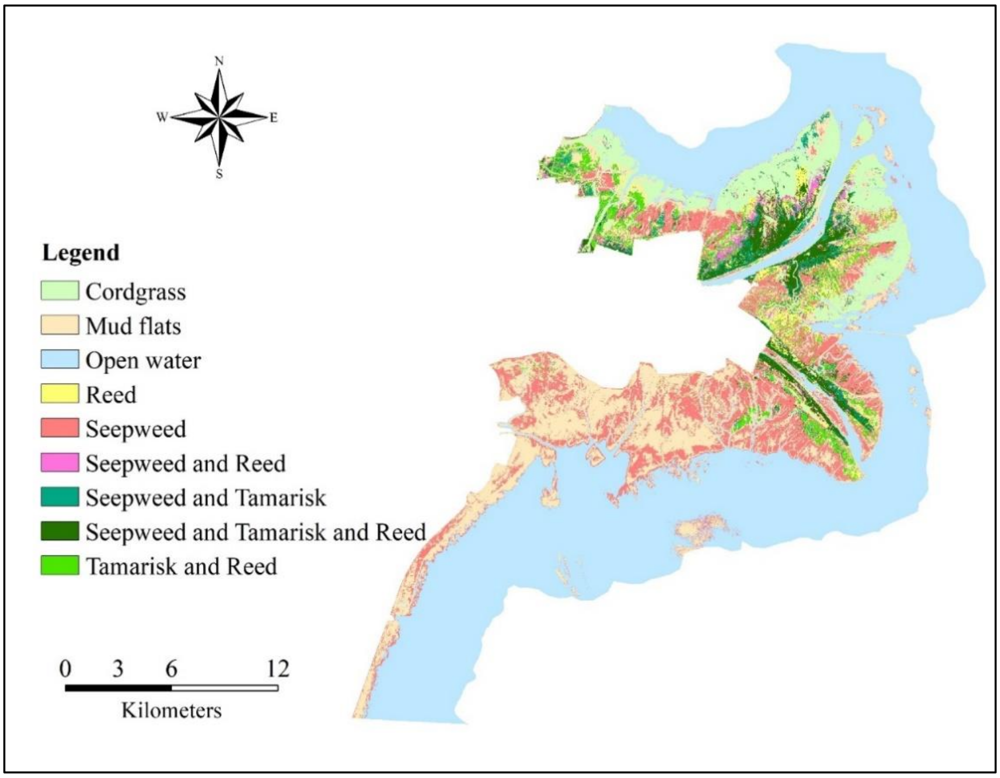

Figure 14 The map of intertidal plant communities produced using winter Sentinel-2 image

Table 8 Confusion matrix for nine-categories plant communities and non-vegetation landscapes classification derived from winter Sentinel-2 image

Prediction	Reference 1	2	3	4	5	6	7	8	9	User's accuracy（%）
1-Cordgrass	**14**	0	0	1	0	1	0	0	0	87.50
2-Mud flats	1	**8**	1	0	4	2	2	0	0	44.44
3-Open water	0	0	**17**	0	0	0	0	0	0	100.00
4-Reed	0	2	0	**7**	0	2	0	1	3	46.67
5-Seepweed	0	9	0	0	**11**	0	1	1	0	50.00
6-Seepweed+Reed	0	1	0	2	1	**7**	1	2	1	46.67
7-Seepweed+Tamarisk	0	0	0	1	2	1	**10**	3	5	45.45
8-Seepweed+Tamarisk+Reed	0	0	0	3	0	1	2	**12**	0	66.67
9-Tamarisk+Reed	0	0	0	0	0	0	0	1	**4**	80.00
Producer's accuracy （%）	93.33	40.00	94.44	50.00	61.11	50.00	62.50	60.00	30.77	
							Overall accuracy	60.81%		
							Kappa	0.57		

3.2. Mapping intertidal plant communities using multi-season Sentinel-2 images

Multi-season consisting of above four single-date images were used to explore the combination of multi-temporal images. The overall classification accuracy from this scenario was 70.07% ± 0.66, and the kappa coefficient was 0.66 ± 0.04. The classification map was shown in Figure 15 while the confusion matrix is in Table 9.

According to the classification result, the class of 3-Open water (producer's accuracy = 94.44%, user's accuracy = 100%) was well performed and classified which only one reference point was misclassified to 2-Mud flats and remaining were all correct. However, the classes of 5-Seepweed (producer's accuracy = 72.22%, user's accuracy = 61.90%) and 6-Seepweed+Reed (producer's accuracy = 71.43%, user's accuracy = 62.50%) were both confused with each other. And the class of 8-Seepweed+Tamarisk+Reed were mostly misclassified to 6-Seepweed+Reed and 7-Seepweed+Tamarisk.

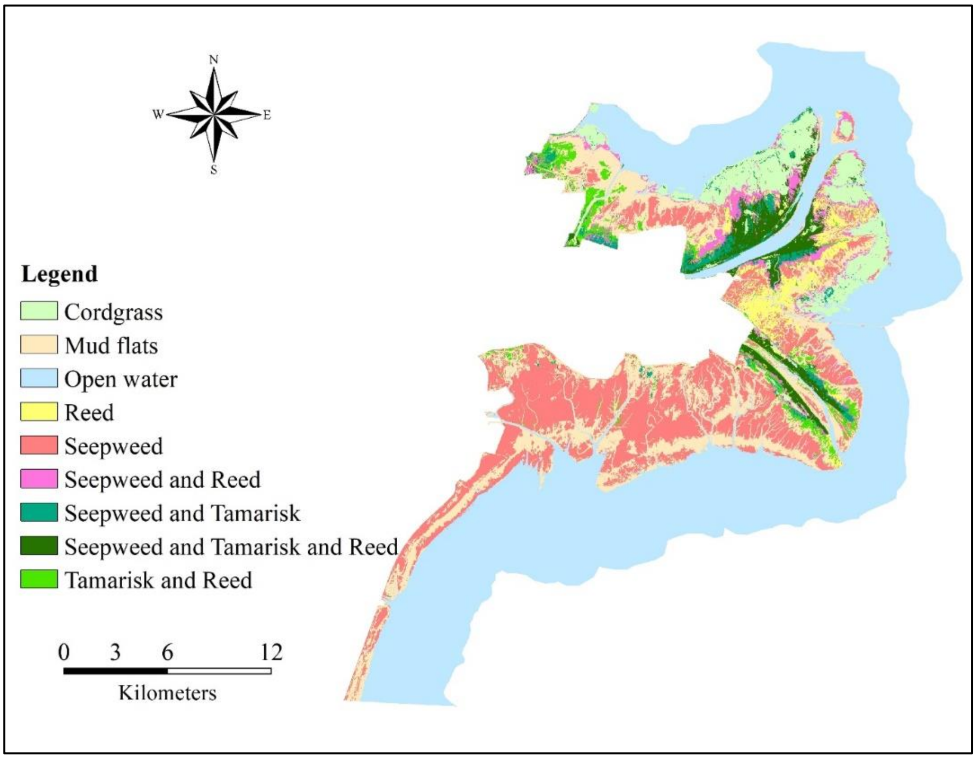

Figure 15 The map of intertidal plant communities produced using multi-season Sentinel-2 images

Table 9 Confusion matrix for nine-categories plant communities and non-vegetation landscapes classification derived from multi-season Sentinel-2 images

Prediction	Reference 1	2	3	4	5	6	7	8	9	User's accuracy (%)
1-Cordgrass	**13**	0	0	1	0	0	0	1	0	86.67
2-Mud flats	1	**14**	1	0	3	0	0	0	0	73.68
3-Open water	0	0	**17**	0	0	0	0	0	0	100.00
4-Reed	0	2	0	**12**	0	2	0	0	1	70.59
5-Seepweed	0	4	0	0	**13**	2	1	1	0	61.90
6-Seepweed+Reed	0	0	0	0	1	**10**	1	2	2	62.50
7-Seepweed+Tamarisk	1	0	0	0	0	0	**11**	3	0	73.33
8-Seepweed+Tamarisk+Reed	0	0	0	1	0	0	1	**13**	0	86.67
9-Tamarisk+Reed	0	0	0	0	1	0	2	0	**10**	76.92
Producer's accuracy (%)	86.67	70.00	94.44	85.71	72.22	71.43	68.75	65.00	76.92	
							Overall accuracy	76.35%		
							Kappa	0.73		

3.3. Mapping intertidal plant communities using time series Sentinel-2 images

Adding the remaining monthly time series Sentinel-2 images in one year to scenario 5, the scenario 6 used the aggregation of twelve monthly multi-temporal Sentinel-2 images from July 2016 to July 2017 to further explore the improved multi-temporal optical images. As a result, scenario 6 achieved the overall accuracy of 70.81% ± 3.05% and the kappa coefficient of 0.67 ± 0.03. The classification map was shown in Figure 16 while the confusion matrix is in Table 10.

According to the classification and confusion matrix, the class of 3-Open water (producer's accuracy = 94.44%, user's accuracy = 100%) showed the same result as scenario 5. The confusion classification appeared in the class of 7-Seepweed+Tamarisk (producer's accuracy = 62.50%, user's accuracy = 66.67%) which around 40% reference points were wrongly predicted into other classes such as 2-Mud flats and 8-Seepweed+Tamarisk+Reed. And the class of 8-Seepweed+Tamarisk+Reed (producer's accuracy = 65.00%, user's accuracy = 86.67%) shows the confusion with the class of 7-Seepweed+Tamarisk.

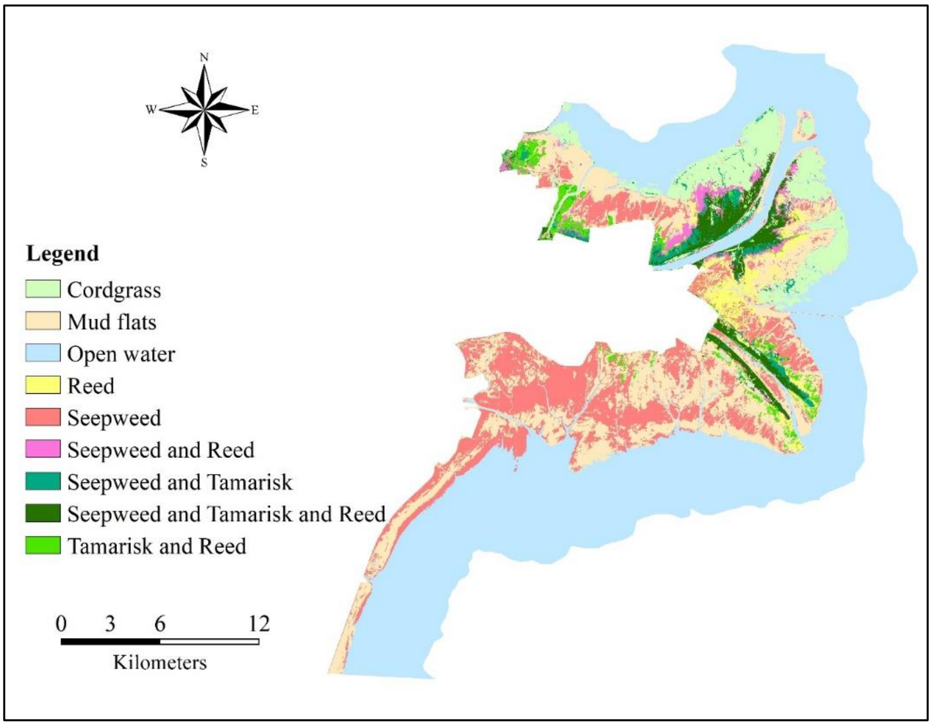

Figure 16 The map of intertidal plant communities produced using time series Sentinel-2 images

Table 10 Confusion matrix for nine-categories plant communities and non-vegetation landscapes classification derived from time series Sentinel-2 images

Prediction	Reference 1	2	3	4	5	6	7	8	9	User accuracy (%)
1-Cordgrass	**13**	0	0	1	0	0	0	1	0	86.67
2-Mud flats	1	**15**	0	0	3	2	2	0	1	62.50
3-Open water	0	0	**17**	0	0	0	0	0	0	100.00
4-Reed	0	2	0	**10**	0	1	0	0	1	71.43
5-Seepweed	0	3	1	0	**14**	0	1	1	0	70.00
6-Seepweed+Reed	0	0	0	1	1	**11**	1	1	2	64.71
7-Seepweed+Tamarisk	1	0	0	0	0	0	**10**	4	0	66.67
8-Seepweed+Tamarisk+Reed	0	0	0	1	0	0	1	**13**	0	86.67
9-Tamarisk+Reed	0	0	0	1	0	0	1	0	**9**	81.82
Producer accuracy (%)	86.67	75.00	94.44	71.43	77.78	78.57	62.50	65.00	69.23	
							Overall accuracy	75.68%		
							Kappa	0.74		

3.4. Mapping intertidal plant communities using NDVI statistic parameters derived from time series Sentinel-2 images

The overall accuracy (54.26% ± 2.40%) and kappa coefficient (0.48 ± 0.03) showed the limitation of using only NDVI statistic parameters for intertidal plant community classification, the speckle and noise in classification map (shown in Figure 17) may be caused by the confusing information of mixed plant communities within one pixel. The highest user's accuracy and producer's accuracy, presented in Table 11, were appeared in the classes of 1-Cordgrass (producer's accuracy = 73.33%, user's accuracy = 100%) and 3-Open water (producer's accuracy = 94.44%, user's accuracy = 100%) while other classes shows poor classification capabilities, especially in the classes of 4-Reed (producer's accuracy = 21.43%, user's accuracy = 25%), 5-Seepweed (producer's accuracy = 38.89%, user's accuracy = 36.84%), 6-Seepweed + Reed (producer's accuracy = 50.00%, user's accuracy = 35.00%).

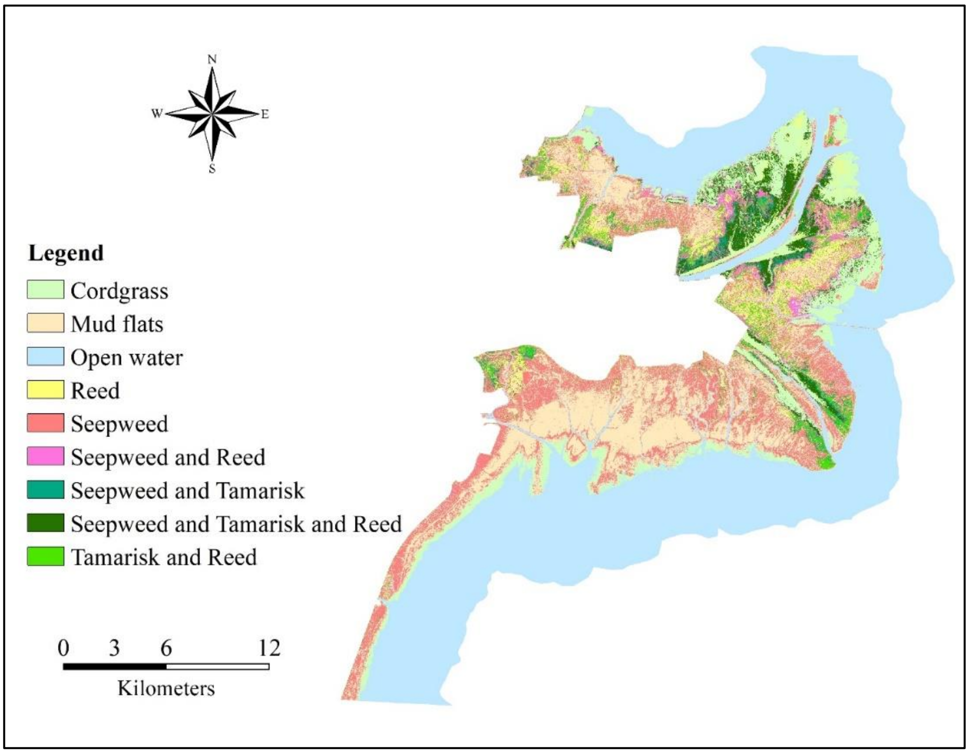

Figure 17 The map of intertidal plant communities produced using NDVI statistical parameters derived from time series Sentinel-2 images

Table 11 Confusion matrix for nine-categories plant communities and non-vegetation landscapes classification derived from NDVI statistic parameters

Prediction	Reference 1	2	3	4	5	6	7	8	9	User accuracy (%)
1-Cordgrass	**11**	0	0	0	0	0	0	0	0	100.00
2-Mud flats	1	**10**	1	1	6	0	0	1	1	47.62
3-Open water	0	0	**17**	0	0	0	0	0	0	100.00
4-Reed	0	1	0	**3**	2	2	3	0	1	25.00
5-Seepweed	0	9	0	0	**7**	2	0	0	1	36.84
6-Seepweed+Reed	1	0	0	6	0	**7**	3	1	2	35.00
7-Seepweed+Tamarisk	0	0	0	1	0	2	**7**	3	0	53.85
8-Seepweed+Tamarisk+Reed	2	0	0	1	0	1	3	**15**	0	68.18
9-Tamarisk+Reed	0	0	0	2	3	0	0	0	**8**	61.54
Producer accuracy (%)	73.33	50.00	94.44	21.43	38.89	50.00	43.75	75.00	61.54	
							Overall accuracy	57.43%		
							Kappa	0.52		

3.5. Mapping intertidal plant communities using time seires Sentinel-2 images and NDVI statistic parameters

Adding the NDVI statistic parameters to time series Sentinel-2 images, scenario 8 achieved the overall accuracy of 70.81% ± 3.05% and the kappa coefficient of 0.67 ± 0.03. And the Figure 18 shows the classification result of scenario 8 and the confusion matrix is shown in Table 12. Being the same as previous scenarios, the best classification appeared in the class of 3-Open water (producer's accuracy = 94.44%, user's accuracy = 100%) while the confusion classifications of 7-Seepweed+Tamarisk (producer's accuracy = 62.50%, user's accuracy = 66.67%) and 2-Mud flats (producer's accuracy = 70.00%, user's accuracy = 60.87%) reflected the limitation of optical time-series images for mapping mixed intertidal plant communities, especially these mixed plant communities which have the common vegetation species.

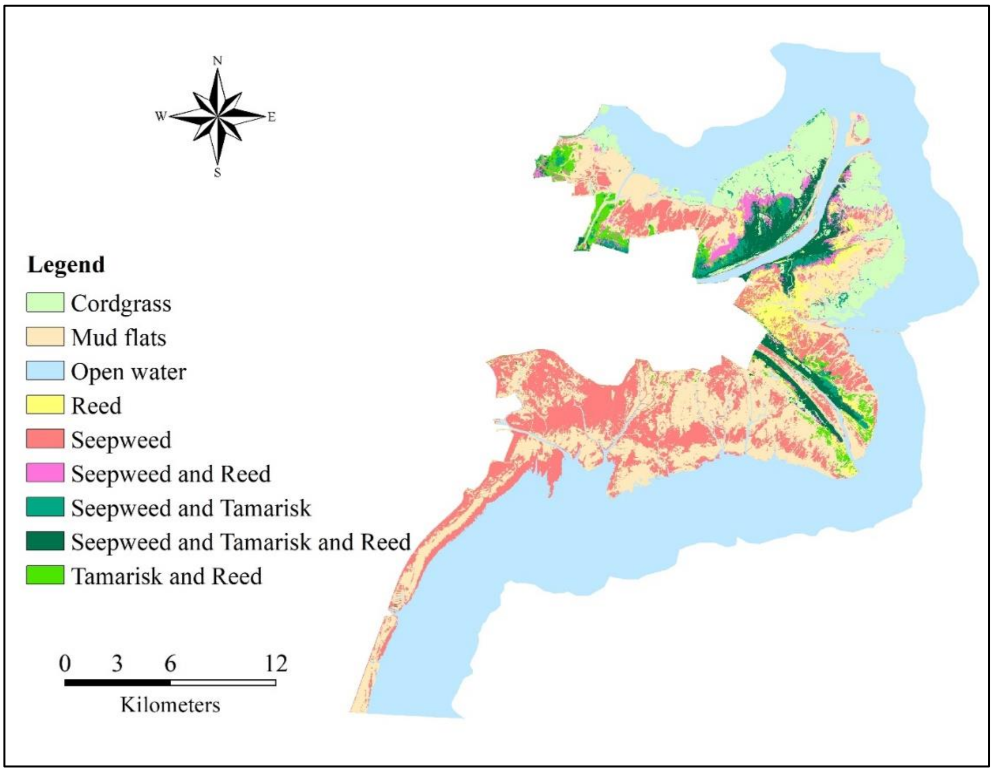

Figure 18 The map of intertidal plant communities produced using time series Sentinel-2 images with NDVI statistical parameters

Table 12 Confusion matrix for nine-categories plant communities and non-vegetation landscapes classification derived from time series Sentinel-2 images with NDVI statistical parameters

Prediction	Reference 1	2	3	4	5	6	7	8	9	User accuracy (%)
1-Cordgrass	**13**	0	0	1	0	0	0	1	0	86.67
2-Mud flats	1	**14**	1	0	3	2	2	0	0	60.87
3-Open water	0	0	**17**	0	0	0	0	0	0	100.00
4-Reed	0	2	0	**12**	0	1	0	0	2	70.59
5-Seepweed	0	3	0	0	**14**	0	1	1	0	73.68
6-Seepweed+Reed	0	0	0	0	1	**11**	1	2	2	64.71
7-Seepweed+Tamarisk	1	0	0	0	0	0	**10**	4	0	66.67
8-Seepweed+Tamarisk+Reed	0	0	0	1	0	0	1	**12**	0	85.71
9-Tamarisk+Reed	0	1	0	0	0	0	1	0	**9**	81.82
Producer accuracy (%)	86.67	70.00	94.44	85.71	77.78	78.57	62.50	60.00	69.23	
							Overall accuracy	75.68%		
							Kappa	0.73		

3.6. Mapping intertidal plant communities using time series Sentinel-1 VV and VH data

The classification result of scenario 9 (the overall accuracy 59.93% ± 3.93% and kappa coefficient 0.55 ± 0.04) was showed in Figure 19, lots of the fragment and noise appeared around land shows the confusing landscape, which reflected the inability when using time series Sentinel-1 VV and VH data. The result showed more confusion classification in most classes, and the obviously confusion appears in the classes of 6-Seepweed+Reed (producer's accuracy = 42.86%, user's accuracy = 54.55%), 7-Seepweed+Tamarisk (producer's accuracy = 43.75%, user's accuracy = 43.75%) and 9-Tamarisk+Reed (producer's accuracy = 46.15%, user's accuracy = 54.55%). Most of the class of 6-Seepweed+Reed was wrongly classified into 5-Seepweed and 7-Seepweed+Tamarisk, while the class of 7-Seepweed+Tamarisk was wrongly classified into 8-Seepweed+Tamarisk+Reed and 9-Tamarisk+Reed.

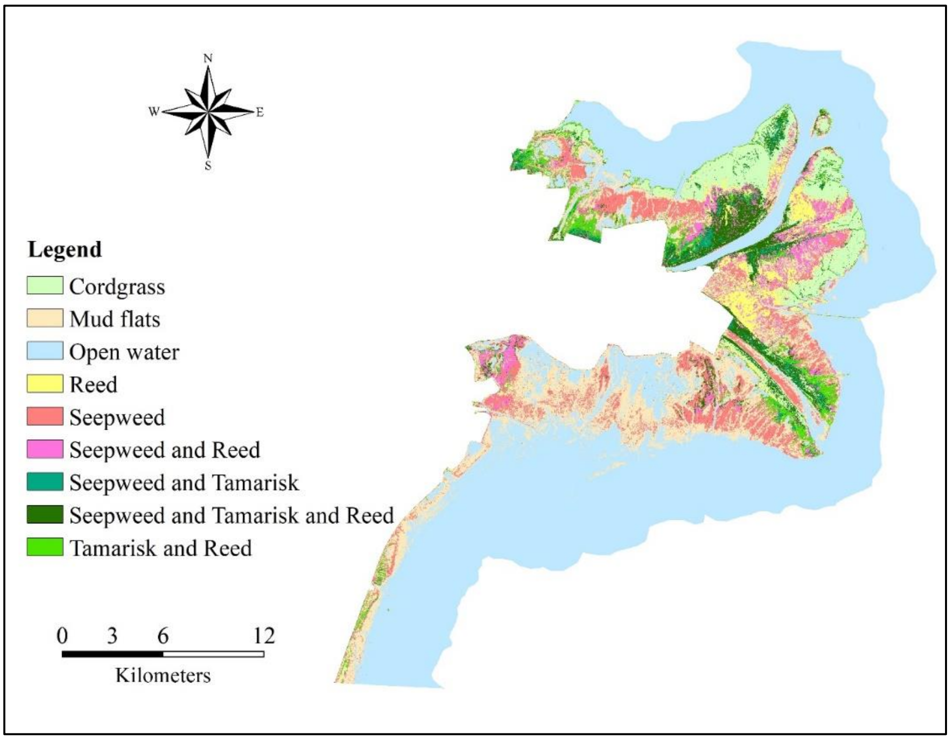

Figure 19 The map of intertidal plant communities produced using time series Sentinel-1 VV and VH images

Table 13 Confusion matrix for nine-categories plant communities and non-vegetation landscapes classification derived from time series Sentinel-1 VV and VH images

Prediction	Reference 1	2	3	4	5	6	7	8	9	User accuracy （%）
1-Cordgrass	**14**	1	0	1	0	0	0	1	0	82.35
2-Mud flats	1	**12**	1	1	2	0	2	0	1	60.00
3-Open water	0	3	**17**	0	0	0	0	0	0	85.00
4-Reed	0	1	0	**10**	0	2	0	1	0	71.43
5-Seepweed	0	1	0	1	**10**	3	0	2	0	58.82
6-Seepweed+Reed	0	1	0	0	1	**6**	1	0	2	54.55
7-Seepweed+Tamarisk	0	0	0	0	1	1	**7**	3	4	43.75
8-Seepweed+Tamarisk+Reed	0	0	0	1	1	2	5	**13**	0	59.09
9-Tamarisk+Reed	0	1	0	0	3	0	1	0	**6**	54.55
Producer accuracy （%）	93.33	60.00	94.44	71.43	55.56	42.86	43.75	65.00	46.15	
							Overall accuracy	64.19%		
							Kappa	0.61		

3.7. Mapping intertidal plant communities using time series Sentinel-2 images, NDVI statistic parameters and time series Sentinel-1 VV and VH data

Figure 20 shows the classification result of plant communities and non-vegetation classes using combination of Sentinel-1 SAR and Sentinel-2 optical time series data with the NDVI statistic parameters derived from the Sentinel-2 time series images. The overall accuracy of scenario 10 is 72.97% ± 3.66% and the kappa coefficient is 0.70 ± 0.04. The confusion matrix, shown in Table 14, presented rather good performance and got relatively high user's accuracy and producer's accuracy, especially in the classes of 1-Cordgrass (producer's accuracy = 86.67%, user's accuracy = 92.86%), 3-Open water (producer's accuracy = 94.44%, user's accuracy = 100%), 8-Seepweed+Tamarisk+Reed (producer's accuracy = 70.00%, user's accuracy = 82.35%) and 9-Tamarisk+Reed (producer's accuracy = 76.92%, user's accuracy = 90.90%). On the other hand, the classes of 7-Seepweed+Tamarisk (producer's accuracy = 56.25%, user's accuracy = 64.29%) and 6-Seepweed+Reed (producer's accuracy = 78.57%, user's accuracy = 68.75%).

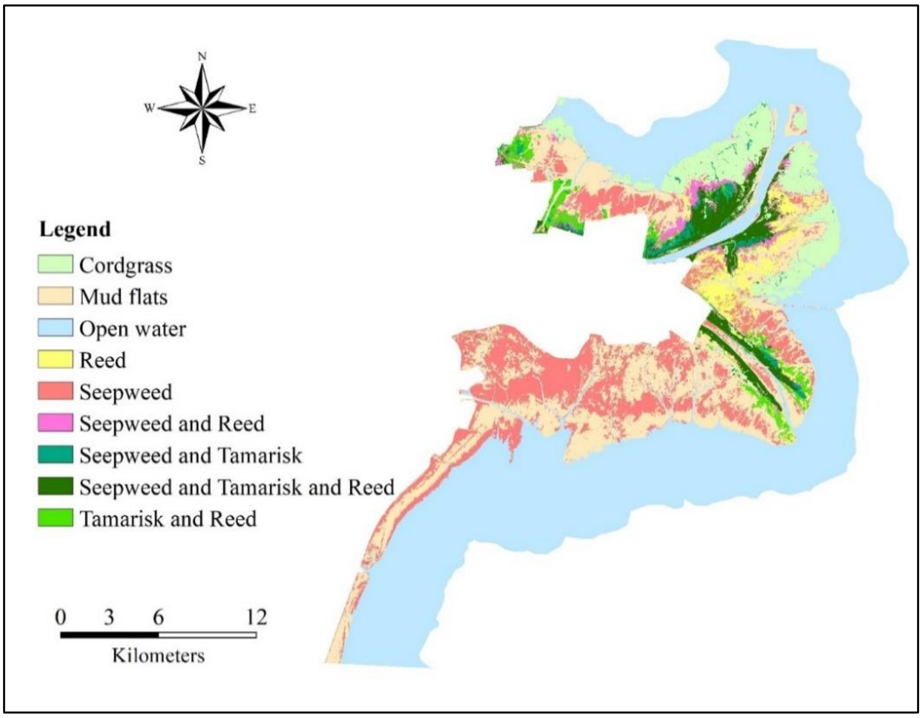

Figure 20 The map of intertidal plant communities produced using time series Sentinel-1 and Sentinel-2 images with NDVI statistical parameters

Table 14 Confusion matrix for nine-categories plant communities and non-vegetation landscapes classification derived from time series Sentinel-1 and Sentinel-2 images with NDVI statistical parameters

	Reference									User
Prediction	1	2	3	4	5	6	7	8	9	accuracy （%）
1-Cordgrass	**13**	0	0	1	0	0	0	0	0	92.86
2-Mud flats	1	**16**	0	1	3	2	2	0	0	64.00
3-Open water	0	0	**17**	0	0	0	0	0	0	100.00
4-Reed	0	1	0	**11**	0	1	0	0	1	78.57
5-Seepweed	0	3	1	0	**14**	0	1	1	0	70.00
6-Seepweed+Reed	0	0	0	0	1	**11**	1	1	2	68.75
7-Seepweed+Tamarisk	1	0	0	0	0	0	**9**	4	0	64.29
8-Seepweed+Tamarisk+Reed	0	0	0	1	0	0	2	**14**	0	82.35
9-Tamarisk+Reed	0	0	0	0	0	0	1	0	**10**	90.90
Producer accuracy （%）	86.67	80.00	94.44	78.57	77.78	78.57	56.25	70.00	76.92	
							Overall accuracy	77.70%		
							Kappa	0.75		

3.8. Comparing the intertidal plant communities mapping accuracies derived from ten models

The boxplots of the overall accuracy and kappa coefficient are shown in Figure 21 in sort of the value from high to low. Table 15 – 17 shows the statistical overall accuracy and kappa coefficient of ten classification scenarios using random forest algorithm.

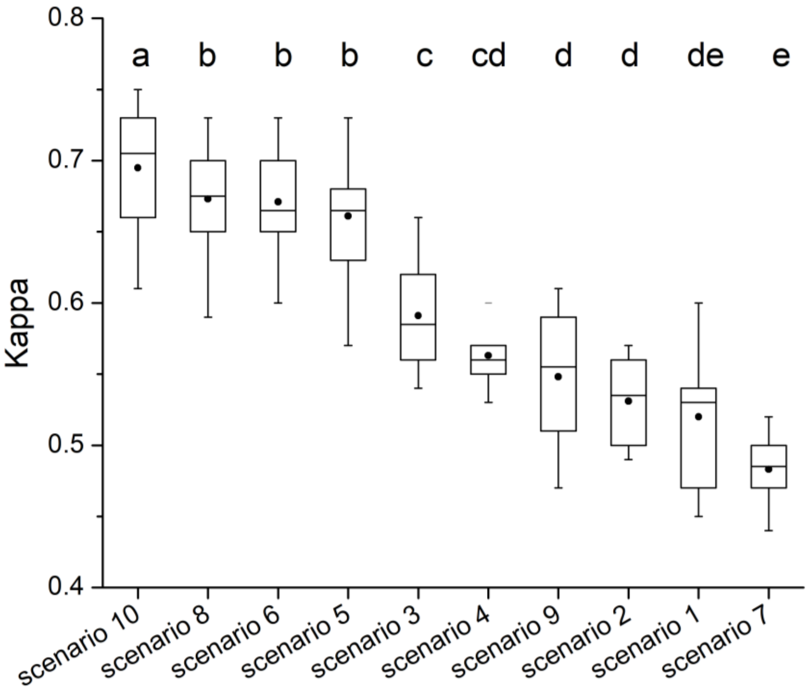

Figure 21 The kappa coefficient of ten scenarios with ten repetitions is shown by box plots (models sorted by the value from high to low). Level of significant difference (a-e) is annotated based on pairwise two-sample t-tests ($p < 0.05$)

In general, the boxplot of overall accuracy presents the same trend as kappa coefficient. Using single-date image of Sentienl-2 could not generate desirable plant communities map (scenario 1: overall accuracy = 57.36% ± 4.22%, kappa coefficient = 0.52 ± 0.05; scenario 2: overall accuracy = 58.51% ± 2.71%; kappa coefficient = 0.53 ± 0.03; scenario 3: overall accuracy = 63.58% ± 3.03%, kappa coefficient = 0.59 ± 0.04; scenario 4: overall accuracy = 61.28% ± 2.03%, kappa coefficient = 0.56 ± 0.02). And the same situation also occurs when use the NDVI statistic parameters (scenario 7: overall accuracy = 54.26% ± 2.40%, kappa coefficient = 0.48 ± 0.03) extracted from Sentinel-2 time series data, and the time series Sentinel-1 VV and VH data (scenario 9: overall accuracy = 59.93% ± 3.93%, kappa coefficient = 0.55 ± 0.04). However, using multi-season Sentinel-2 images (scenario 5: overall accuracy = 70.07% ± 3.79%, kappa coefficient = 0.66 ± 0.04), Sentinel-2 time series images (scenario 6: overall accuracy = 70.81% ± 3.05%, kappa coefficient = 0.67 ± 0.03) and Sentinel-2 time series data combined with NDVI statistical parameters (scenario 8: overall accuracy = 70.81% ± 3.35%, kappa coefficient = 0.67 ± 0.04) performed much better than previous scenarios. Moreover, high overall accuracy can be achieved by using integration of multi-sensor images. The integration of time series Sentinel-1 and Sentinel-2 images (scenario 10: overall accuracy = 72.97% ± 3.66%, kappa coefficient = 0.70 ± 0.04) were proven to be best classification scenario in mapping intertidal plant communities.

Table 15 shows the significant difference between ten scenarios' kappa coefficient with each other. In Figure 21 above the boxplot shows the level of significant difference (a - e) annotated based on pairwise two-sample t-tests with 95% confidence interval. Interpretably, the integration of Sentinel-1 SAR and Sentinel-2 optical time series images with the NDVI statistic parameters (scenario 10) not only achieved the best classification accuracy but also shows the significant difference with other scenarios, which proves their complementary information contained in optical and SAR images. It means the intertidal plant communities could benefit from the distinctive features of Sentinel-1 SAR and Sentinel-2 optical data. Optical sensors receive the reflectance spectrum from ground objects and contain information on surface reflectance and emissivity characteristics, while SAR captures the structure and dielectric properties of the Earth surface materials, and provide the information on water content, texture and characteristics. Land cover types, in this study, especially vegetation types that are impossible to separate in optical images might be distinguishable with SAR images and vice versa. Interestingly, the classification with integrated Sentinel-2 time series images and NDVI statistic parameters (scenario 8) showed no significant difference in the accuracy assessment compared with using only Sentinel-2 time series data and multi-season Sentinel-2 images, which means the statistical metrics derived from multi-temporal NDVI data into the classification did not contribute to improving the mapping accuracy. The reason might lie in the confusion of mixed plant communities within one pixel. Furthermore, the results showed weak capability for the single-date image (scenario 1 to scenario 4), individual NDVI statistical parameter (scenario 7) and Sentinel-1 time series VV and VH data (scenario 9). For the single-date image, the information was limited by the moment of the image was shot, leading to confusing and non-distinctive spectral reflectance. NDVI statistical parameters derived from Sentinel-2 time series data limited by the confusion of mixed plant communities within one pixel, while the Sentinel-1 time series VV and VH were limited by the acquisition time. For Sentinel-1, the sensor-acquired the images during the flood phase, in which most of the plant communities were submerged at high tide, leading an underestimation of vegetated area.

Table 15 The significant difference between kappa coefficient of ten scenarios with 95% confidence interval

Model	1	2	3	4	5	6	7	8	9	10
1		*	**	**	****	****	****	****	****	****
2			ns	ns	****	****	****	****	****	****
3				ns	****	****	****	****	****	****
4					***	****	****	****	****	****
5						ns	**	**	***	****
6							ns	*	*	****
7								ns	ns	**
8									ns	***
9										ns
10										

Table 16 The statistical overall accuracy of ten scenarios

Model	Overall accuracy			
	Min	Mean	Max	Standard deviation
1	51.35%	57.36%	64.19%	4.22%
2	54.73%	58.51%	62.16%	2.71%
3	59.46%	63.58%	69.59%	3.03%
4	58.11%	61.28%	64.86%	2.03%
5	62.16%	70.07%	76.35%	3.79%
6	64.19%	70.81%	75.68%	3.05%
7	50.68%	54.26%	57.43%	2.40%
8	64.19%	71.08%	75.68%	3.35%
9	53.38%	59.93%	65.54%	3.93%
10	65.54%	72.97%	77.70%	3.66%

Table 17 The statistical kappa coefficient of ten scenarios

Model	Kappa coefficient			
	Min	Mean	Max	Standard deviation
1	0.45	0.52	0.60	0.05
2	0.49	0.53	0.57	0.03
3	0.54	0.59	0.66	0.04
4	0.53	0.56	0.60	0.02
5	0.57	0.66	0.73	0.04
6	0.60	0.67	0.73	0.03
7	0.44	0.48	0.52	0.03
8	0.59	0.67	0.73	0.04
9	0.47	0.55	0.61	0.04
10	0.61	0.70	0.75	0.04

3.9. Importance of the variables

Variable importance was estimated by the Gini index acquired from random forest algorithm, and it indicated the significance of input data in different combination. The overall important variables were selected to display in the following figure. Figure 22 presents the variable importance and ranking of the selected Sentinel-1, Sentinel-2 and NDVI statistical metrics for the best classification scenario (scenario 10) among ten scenarios bases on the Gini index.

It is not difficult to find that not all the variables performed equally in the classification results. The first ten variables presented high contribution for plant communities classification. As shown in Figure 22, three red edge bands (band 5,6,7) from the image captured on a certain date of October 14, 2016 appeared as the first-ranked metrics under the condition for mapping intertidal plant communities, followed by the mean statistical NDVI data. Moreover, the images acquired in September, October, December contributed most among all images, and the images acquired in the season of early autumn provided most significant information and contribution for plant communities in the intertidal zones of the Yellow River Delta. The reason may lie in the growth stage of the plant communities grown in the study area. In the early autumn plant species are maturing, some distinctive characteristics reflected through radiation and captured by the satellite sensors; seepweeds are turning to be red color, cordgrass are yellowing, while reed catkins are growing white. Red edge bands are very sensitive to the chlorophyll content change in vegetation especially in autumn. Generally, according to the figure, multi-temporal Sentinel-1 images were less important for mapping plant communities in the intertidal zones compared with multi-temporal Sentinel-2 images.

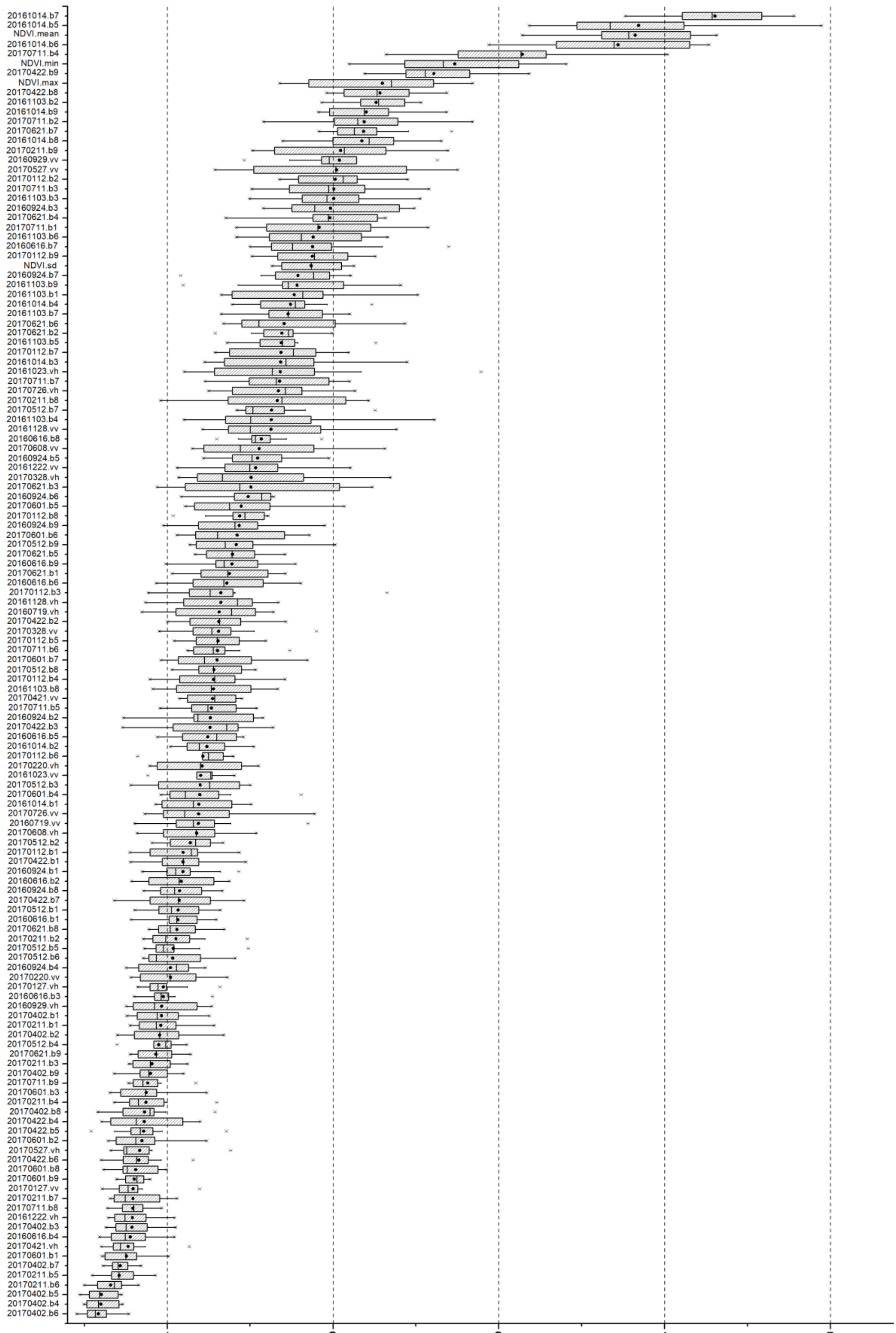

Figure 22 Random Forest classification variable importance under scenario 10; the Mean Decrease Gini index. All 136 variables are sorted in ascending order according to their median importance in the model after 10 runs.

4. DISCUSSION

4.1. Mapping plant communities using single-date Sentinel-2 images

In this study, seven plant communities, consisting of different single and mixed plant species, and two non-vegetation classes were successfully distinguished and classified using remotely sensed data. Optical data were proposed for wetland identification and vegetation detection. Various applications and classification methods of the satellite remote sensing (i.e., Landsat MSS, Landsat TM, SPOT, AVHRR, IRD-1B and LISS-II) were summarized (Gómez et al., 2016; Ozesmi & Bauer, 2002). To get over the difficulties caused by the similarities of spectral reflectance contributed by the same basic components such as chlorophyll, carotene and other light-absorbing pigments and to improve the classification accuracy of plant communities, multi-temporal Sentinel-2 images were explored the ability for mapping plant communities. However, lots of studies also showed successful classification of wetland vegetation and landscape through the single-date image. Therefore, it is worthing exploring the classification capability of both single-date and multi-temporal images for distinguishing and mapping the intertidal plant communities in the Yellow River Delta. The results of scenarios with multi-temporal optical images revealed phenological characteristics of plant communities in highly dynamic wetland landscape. On the contrast, the scenarios with single-date images did not.

Because the plant species in the intertidal zones of the Yellow River Delta are annual plants, the multi-temporal Sentinel-2 images were selected monthly images acquired from July 2016 to July 2017 for providing distinctive phenological characteristics. And four single-date images, which were captured on April 22 of 2017, July 11 of 2017, October 14 of 2016 and January 12 of 2017, was selected as the representatives of different seasons according to the season distinction based on the average monthly temperature and rainfall for Dongying City from the year of 1971 to 2000. Through the accuracies comparison, the season of autumn (scenario 3: overall accuracy = 63.58% ± 3.03%, kappa coefficient = 0.59 ± 0.04) was proven to be the better season which significantly contributed more to the classification accuracy than others (scenario 1-spring: overall accuracy = 57.36% ± 4.22%, kappa coefficient = 0.52 ± 0.05; scenario 2-summer: overall accuracy = 58.51% ± 2.71%; kappa coefficient = 0.53 ± 0.03; scenario 4-winter: overall accuracy = 61.28% ± 2.03%, kappa coefficient = 0.56 ± 0.02). The maximum discrepancy on spectral reflectance between different plant species appeared in the season of autumn, making it the optimum season for certain plants classification in the study area. The reason may lie in the growth stage of the plant communities grown in the study area. In the season of autumn plant species are maturing, some distinctive characteristics reflected through radiation and then be captured by the satellite sensors, of which the red edge bands are very sensitive to the chlorophyll content change in vegetation; these distinctive changes may indicate that seepweeds are turning to be red color, cordgrass are yellowing, while reed catkins are growing white in autumn.

It is worth mentioning that salt patches were found in some part of high tide zones, especially in some dry seasons. It was these white salt patches cause the confusion of mud flats and mixed plant communities, resulting in relatively low overall accuracy and low kappa coefficient. The level of tides is influenced by the combined effects of the gravitational forces exerted by the Moon and the Sun as well as the self-rotation of the Earth. The water content of the high tide zones decreases with the high tide line getting lower during autumn and winter, leading to salt precipitation. On the other hand, the confusion matrix shows the same problems, almost half of the class of 2-mud flats were misclassified into plant communities.

Therefore, the salt patches make it difficult distinguishing and classifying the mud flats covered by salt. The selected season of the single-date image could also influence the mapping accuracy and classification results. Therefore, caution should be exercised when mapping highly dynamic landscape with single-date data, especially in the dry seasons.

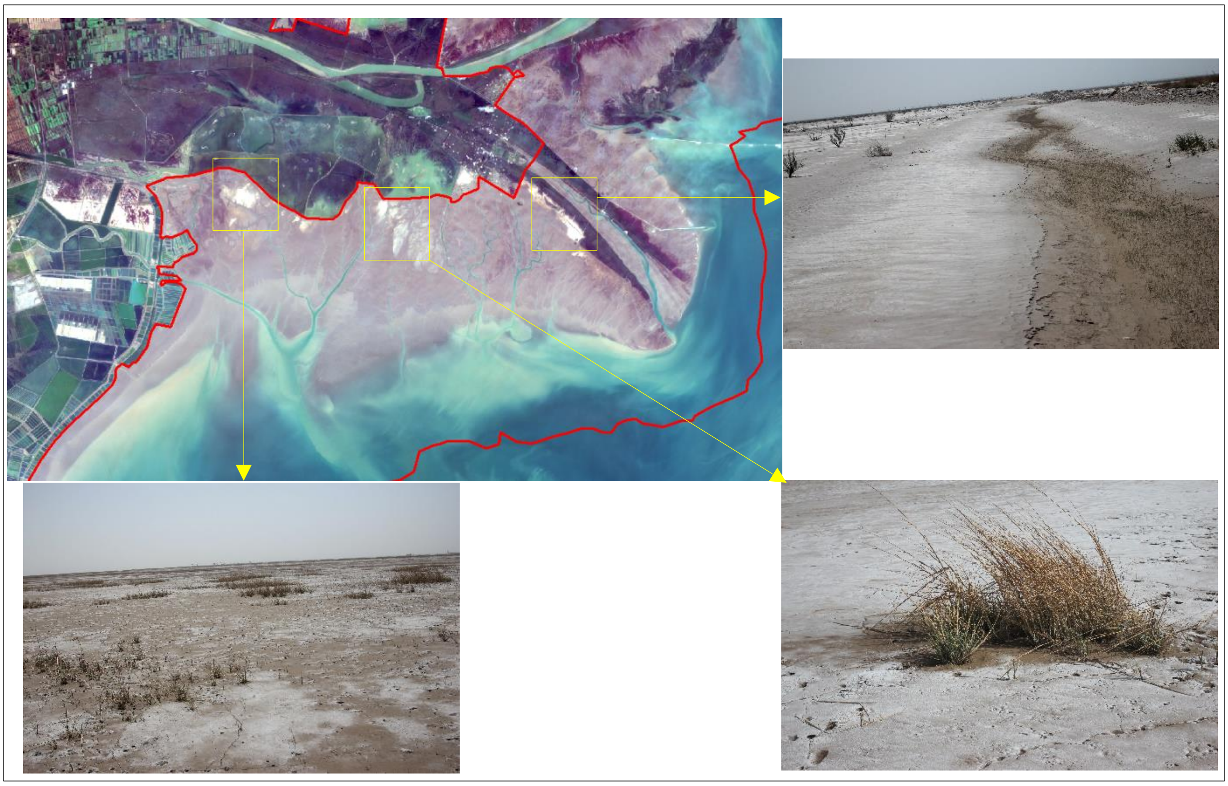

Figure 23 The salt patch found in the high tide zones

4.2. Mapping plant communities using multi-temporal Sentinel-2 data

In this study, two scenarios (i.e., scenario 5 and scenario 6) were implemented to explore the capability for classifying and mapping the intertidal plant communities in the Yellow River Delta in the temporal dimension. Scenario 5 aggregated the four single-date Sentinel-2 images to form the multi-season Sentinel-2 images while Scenario 6 aggregated the twelve-monthly single-date Sentinel-2 images to form the Sentinel-2 time series data.

The classification results of scenario 5 (overall accuracy = 70.07% ± 3.79%, kappa coefficient = 0.66 ± 0.04) and scenario 6 (overall accuracy = 70.81% ± 3.05%, kappa coefficient = 0.67 ± 0.03) shows that there is no significant difference between each other. This situation was not difficult to explain when taking the variable importance into consideration. According to Figure 22, it was found that among the top fifteen variables, nine of them were included in the scenario 5 and twelve variables (including the variables in the scenario 5 but except for the NDVI statistical parameters) were included in the scenario 6, which means that scenario 5 contained the most important variables with a large proportion of contribution to mapping accuracy even though it contained a less amount of images than scenario 6. In other words, even though scenario 6 had more time series data than scenario 5, the extra data were of less significance and may not make a significant difference between these two scenarios. Therefore, the suggestion can be concluded that multi-season Sentinel-2 images which aggregated four single-date images captured in January, April, July and October were adequate for mapping intertidal plant communities in this study area and adding other multi-temporal Sentinel-2 images cannot significantly improve the overall mapping accuracy and kappa coefficient.

According to the confusion matrix, the classes of 6-Seepweed+Reed and 7-Seepweed+Tamarisk were confused with each other and the class of 5-Seepweed was confused with the class of 2-Mud flats for both scenarios. And the prediction of the class of 2-Mud flats was partly from mixed plant communities, while some of the 9-Tamarisk+Reed were misclassified into the classes of 6-Seepweed+Reed and 4-Reed, which means the distinguishing and classifying of mixed plant communities of the intertidal zones still need improvement.

4.3. Mapping plant communities when adding the NDVI statistical parameters

The NDVI statistical parameters are proposed to be used for wetland mapping (Halabuk & Mojses, 2015; Nageswara et al., 2005; Tucker, 1979). In this study, the NDVI statistical parameters were generated from the Sentinel-2 time series data which as the feature derived from multi-temporal optical images. Scenario 7 used the only NDVI statistical parameters as the input variables while scenario 8 adding the NDVI statistical parameters into Sentinel-2 time series data as the auxiliary data. The classification results of scenario 7 (overall accuracy = 54.26% ± 2.40%, kappa coefficient = 0.48 ± 0.03) and scenario 8 (overall accuracy = 70.81% ± 3.35%, kappa coefficient = 0.67 ± 0.04) showed large difference between these two scenarios. And the performance of scenario 7 was ranking the last classification among ten different combinations of input variables, which presented that the single NDVI statistical parameters had the inability for mapping intertidal plant communities in this study. As for scenario 8, the paired t-test shows that there is no significant difference between scenario 8 and scenario 6, which means that adding vegetation index statistical parameters based on the Sentinel-2 time series data did not contribute to significantly improving the mapping accuracy. The reason might lie in the confusion of mixed plant communities within one pixel.

However, shown in Figure 22, three parameters (i.e., mean, minimum and maximum) were respectively ranking 3rd, 6th, 9th important among the most significant fifteen input variables for mapping intertidal plant communities in the Yellow River Delta. It seemed that the NDVI statistical parameters played an important role as auxiliary data when mapping intertidal plant communities but could not be used as single input data. The confusion matrix showed the poor capability for distinguishing 4-Reed and 6-Seepweed+Reed. Also, the class of 5-Seepweed were mostly misclassified into 2-Mud flats. The reason may lie in the chlorophyll content in vegetation and the variation. For the seepweed, it grows to be red in the autumn with the decreasing chlorophyll content, leading the seasonal variation of NDVI value of the 5-Seepweed class similar to 2-Mud flats in autumn and winter, which lead to the confusion of these two classes.

4.4. Mapping plant communities using integretion of Sentinel-1 SAR and Sentinel-2 optical timre series data

The Sentinel-1 time series data with dual VV and VH polarization (scenario 9) were used as input variables for mapping intertidal plant communities in the Yellow River Delta. The classification results achieved the overall accuracy of 59.93% ± 3.93% and the kappa coefficient of 0.55 ± 0.04, reflecting the less capability for distinguishing and classification intertidal plant communities compared with Sentinel-2 time series data. The classification map and confusion matrix showed the confusion of 3-Open water and 2-Mud flats. According to the Figure 19, it was found that in the south of the study area, a large extent was classified into the class of 3-Open water; as well as the northwest part of the study area. Moreover, the classes of 6-Seepweed+Reed and 7-Seepweed+Tamarisk were largely misclassified into 8-Seepweed+Tamarisk+Reed. Also, the class of 9-Tamarisk+Reed were mostly misclassified into the classes of 6-Seepweed+Reed and 7-Seepweed+Tamarisk. A plausible explanation seems to be that the intertidal wetland landscape was highly dynamic, and the characteristics of the plant communities shown in Sentinel-1 time series images might not match the ground truth data due to the time difference of satellite passing the study area. For Sentinel-1, the sensor-acquired the images during the flood phase, in which most of the plant communities were submerged at high tide; by contrast, the ground truth data were collected during the ebb phase and most of the plant communities were exposed to the air at low tide. Therefore, the integration of Sentinel-1 data caused an underestimation of vegetated area.

Many researches using both optical and SAR images have been explored for land cover classification (Amarsaikhan & Douglas, 2004; Blaes et al., 2005; Chust et al., 2004) and most of the results from integrating optical and SAR sensors are always significantly higher than those obtained from using an individual sensor, particularly for certain land cover types, such as urban (Corbane et al., 2008; Toll, 1985) agriculture (Blaes et al., 2005; Chust et al., 2004) and wetlands (Augusteijn & Warrender, 1998b; Li & Chen, 2005). As mentioned literatures, Scenario 10 integrated the Sentinel-1 time series data and the Sentinel-2 time series data combined with features extracted by statistical metrics of multi-temporal vegetation index, obtaining a significantly higher overall accuracy of 72.97% $\pm$ 3.66% and the kappa coefficient of 0.70 $\pm$ 0.04 than others. According to the variable importance, the results of scenario 10 has the significant difference between others, showing the best performance among all the scenarios. That was because SAR images captured the structure and dielectric properties of the intertidal plant communities, providing the complementary information which could not be derived from Sentinel-2 time series data. However, the confusion matrix reflected the limitation for distinguishing and classifying the mixed plant communities such as the classes of 7-Seepweed+Tamarisk and 6-Seepweed+Reed, some of them are misclassified into the class of 8-Seepweed+Tamarisk+Reed. The reason may lie in the confusion spectral reflectance of mixed plant communities and less distinctive vegetation phonologies.

5. CONCLUSION AND RECOMMENDATIONS

5.1. Conclusions

This study fulfils the classification and mapping plant communities in the intertidal zones of the Yellow River Delta based on the techniques of remote sensing and geographic information system. The intertidal zones are highly dynamic wetland ecosystem with spectral mixture among plant species, making it difficult distinguishing and mapping the plant communities submerged at high tide. Traditional vegetation mapping requires field investigation including visual inspection, field measurement and date record, which need lots of expertise on plant taxonomy. In reduce the amount of filed work and obtain accurate information on spatial distribution and classification of intertidal plant communities, optical and SAR images have an approach to capture all the inherent seasonal variance of plant phenology, and are explored providing basic information on texture, feature, and characteristic of vegetation species. In this study, three aspects have been explored corresponding to the research objectives: a) use single-date images of Sentinel-2 for mapping plant communities in the intertidal zones; b) use multi-season and time series Sentinel-2 images with or without the NDVI statistical parameters derived from Sentinel-2 time series data c) use integrations of Sentinel-1 SAR and Sentinel-2 optical time series images.

The specific conclusions drawn from this study can be summarized as follows:

- The mapping accuracies of the single-date images captured in the seasons of spring (overall accuracy = 57.36% ± 4.22%, kappa coefficient = 0.52 ± 0.05) and summer (overall accuracy = 58.51% ± 2.71%; kappa coefficient = 0.53 ± 0.03) were significantly lower than the results of the seasons of autumn (overall accuracy = 63.58% ± 3.03%, kappa coefficient = 0.59 ± 0.04) and winter (overall accuracy = 61.28% ± 2.03%, kappa coefficient = 0.56 ± 0.02). The season of autumn performed best among all seasons due to the distinctive characteristics of various vegetation species.

- The aggregated multi-season Sentinel-2 images with the overall accuracy of 70.07% ± 3.79% and kappa coefficient of 0.66 ± 0.04 significantly improve the mapping accuracy and kappa coefficient based on using the single-date images through paired t-test. It concluded that the multi-temporal Sentinel-2 images can significantly improve the classification of the intertidal plant communities compared to a single season. Interestingly, the aggregated monthly Sentinel-2 time series images did not significantly improve the mapping accuracy based on using multi-season Sentinel-2 images. A plausible explanation seemed to be that the multi-season Sentinel-2 images contained most variable importance for mapping vegetation in such dynamic wetland and the extra images did not contributed so much in the classification of time series images.

- The NDVI statistical parameters derived from the Sentinel-2 time series data have no capability for mapping the intertidal plant communities by itself, resulting in the worst performance with the overall accuracy of 54.26% ± 2.40% and kappa coefficient of 0.48 ± 0.03. The reason may lie in the confusion of mixed plant communities within one pixel. Moreover, adding the NDVI statistical parameters to the Sentinel-2 time series images achieved a mean overall accuracy of around 70.81% with a mean kappa coefficient of around 0.67, which did not significantly improve the mapping accuracy than the scenario without the NDVI statistical parameters.

- Using the combination of Sentinel-1 SAR and Sentinel-2 optical time series images can significantly improve the mapping accuracy of the plant communities in the intertidal zones, obtaining a significantly higher overall accuracy of 72.97% ± 3.66% and the kappa coefficient of 0.70 ± 0.04 based on other combination of input variables. However, the classification results (overall accuracy = 59.93% ± 3.93%, kappa coefficient = 0.55 ± 0.04) showed the inability for classification when using the individual Sentinel-1 time series data, due to the time of satellites passing the study area was during the flood phase while other images were captured during ebb phase. Therefore, caution should be exercised when mapping highly dynamic landscape with multi-sensor data acquired at a different time during a day, particularly when land covers may change rapidly with daily tides.

5.2. Recommendations

Wetlands play an important role in a natural ecosystem, especially for the globally important area. The plant communities in the intertidal zones of the Yellow River Delta were statistically analysed with random forest algorithm. In this research, the final map and accuracy assessment were based on ten-fold classification of ten different combinations of input variables. The number of training and validating samples for mapping intertidal plant communities was limited by the poor accessibility of study area, causing more uncertainty in the classification results. And the time difference for Sentinel-1 and Sentinel-2 being captured caused overestimation of open water because they could not match each other in the daily tide phase.

For further research, the combination of ground observations and UAV technique can provide a more scientific approach for overcoming the poor accessibility during field work. The sample points collected by UAV technique can be interpreted through relevant methods to ensure the quality of ground truth data. And caution should be exercised when mapping highly dynamic landscape with multi-sensor data acquired at a different time during a day, particularly when land covers may change rapidly with daily tides. It is also suggested to use the combination of optical and SAR images during the same phase in such intertidal zones.

LIST OF REFERENCES

Abdel-Rahman, E. M., Mutanga, O., Adam, E., & Ismail, R. (2014). Detecting Sirex noctilio grey-attacked and lightning-struck pine trees using airborne hyperspectral data, random forest and support vector machines classifiers. *ISPRS Journal of Photogrammetry and Remote Sensing*, *88*, 48–59. https://doi.org/10.1016/j.isprsjprs.2013.11.013

Adam, E., Mutanga, O., & Rugege, D. (2010). Multispectral and hyperspectral remote sensing for identification and mapping of wetland vegetation: a review. *Wetlands Ecology and Management*. Retrieved from http://link.springer.com/article/10.1007/s11273-009-9169-z

Amarsaikhan, D., & Douglas*, T. (2004). Data fusion and multisource image classification. *International Journal of Remote Sensing*, *25*(17), 3529–3539. https://doi.org/10.1080/0143116031000115111

Ambrose, W. G. (1986). Estimate of removal rate ofNereis virens (Polychaeta: Nereidae) from an intertidal mudflat by gulls (Larus spp.). *Marine Biology*, *90*(2), 243–247. https://doi.org/10.1007/BF00569134

Archer, K. J., & Kimes, R. V. (2008). Empirical characterization of random forest variable importance measures. *Computational Statistics & Data Analysis*, *52*(4), 2249–2260. https://doi.org/10.1016/J.CSDA.2007.08.015

Augusteijn, M. F., & Warrender, C. E. (1998a). Wetland classification using optical and radar data and neural network classification. *International Journal of Remote Sensing*, *19*(8), 1545–1560. https://doi.org/10.1080/014311698215342

Augusteijn, M. F., & Warrender, C. E. (1998b). Wetland classification using optical and radar data and neural network classification. *International Journal of Remote Sensing*, *19*(8), 1545–1560. https://doi.org/10.1080/014311698215342

Ayyangar, R., Nagaeshwara Rao, P., & Rao, K. (1980). Crop cover and crop phenological information from red and infrared spectral response. *Ind. Soc. Photo-Int. & Remote Sensing*, *8*(1). Retrieved from https://link.springer.com/content/pdf/10.1007/BF02990665.pdf

Baghdadi, N., Gratiot, N., Lefebvre, J.-P., Oliveros, C., & Bourguignon, A. (2004). Coastline and mudbank monitoring in French Guiana: contributions of radar and optical satellite imagery. *Canadian Journal of Remote Sensing*, *30*(2), 109–122. https://doi.org/10.5589/m03-059

Belgiu, M., & Drăguţ, L. (2016). Random forest in remote sensing: A review of applications and future directions. *ISPRS Journal of Photogrammetry and Remote Sensing*, *114*, 24–31. https://doi.org/10.1016/j.isprsjprs.2016.01.011

Belluco, E., Camuffo, M., Ferrari, S., Modenese, L., Silvestri, S., Marani, A., & Marani, M. (2006). Mapping salt-marsh vegetation by multispectral and hyperspectral remote sensing. https://doi.org/10.1016/j.rse.2006.06.006

Bertness, M. D., Gaines, S. D., & Hay, M. E. (2001). Marine Community Ecology. *Coral Reefs*, 550. https://doi.org/10.2307/2679975

Bhandari, A. K., Kumar, A., & Singh, G. K. (2012). Feature Extraction using Normalized Difference Vegetation Index (NDVI): A Case Study of Jabalpur City. *Procedia Technology*, *6*, 612–621. https://doi.org/10.1016/J.PROTCY.2012.10.074

Bhandari, S., Phinn, S., & Gill, T. (2012). Preparing Landsat Image Time Series (LITS) for Monitoring Changes in Vegetation Phenology in Queensland, Australia. *Remote Sensing*, *4*(12), 1856–1886. https://doi.org/10.3390/rs4061856

Blaes, X., Vanhalle, L., & Defourny, P. (1969). *Remote sensing of environment. Remote Sensing of Environment : an interdisciplinary journal* (Vol. 96). American Elsevier Pub. Co. Retrieved from https://dial.uclouvain.be/pr/boreal/object/boreal:39204

Blaes, X., Vanhalle, L., & Defourny, P. (2005). Efficiency of crop identification based on optical and SAR image time series. *Remote Sensing of Environment*, *96*(3–4), 352–365. https://doi.org/10.1016/J.RSE.2005.03.010

Breiman, L. (2001). Random Forests. *Machine Learning*, *45*(1), 5–32. https://doi.org/10.1023/A:1010933404324

Brohman, R. J., Bryant, L. D., Tart, D., Williams, C. K., Brewer, C. K., Dibenedetto, J. P., … Schanta, M. (2005). Existing Vegetation Classification and Mapping Technical Guide Version 1.0. Retrieved from https://www.fs.fed.us/emc/rig/documents/integrated_inventory/FS_ExistingVEG_classif_mapping_TG_05.pdf

Chan, J. C.-W., Beckers, P., Spanhove, T., & Borre, J. Vanden. (2012). An evaluation of ensemble classifiers for mapping Natura 2000 heathland in Belgium using spaceborne angular hyperspectral (CHRIS/Proba) imagery. *International Journal of Applied Earth Observation and Geoinformation*, *18*, 13–22. https://doi.org/10.1016/j.jag.2012.01.002

Chan, J. C.-W., & Paelinckx, D. (2008a). Evaluation of Random Forest and Adaboost tree-based ensemble classification and spectral band selection for ecotope mapping using airborne hyperspectral imagery. *Remote Sensing of Environment*, *112*(6), 2999–3011. https://doi.org/10.1016/j.rse.2008.02.011

Chan, J. C.-W., & Paelinckx, D. (2008b). Evaluation of Random Forest and Adaboost tree-based ensemble classification and spectral band selection for ecotope mapping using airborne hyperspectral imagery. *Remote Sensing of Environment*, *112*(6), 2999–3011. https://doi.org/10.1016/J.RSE.2008.02.011

Chust, G., Ducrot, D., & Pretus, J. L. (2004). Land cover discrimination potential of radar multitemporal series and optical multispectral images in a Mediterranean cultural landscape. *International Journal of Remote Sensing*, *25*(17), 3513–3528. https://doi.org/10.1080/0143116032000160480

Colditz, R., & Roland, R. (2015). An Evaluation of Different Training Sample Allocation Schemes for Discrete and Continuous Land Cover Classification Using Decision Tree-Based Algorithms. *Remote Sensing*, *7*(8), 9655–9681. https://doi.org/10.3390/rs70809655

Congalton, R. G. (1991). A review of assessing the accuracy of classifications of remotely sensed data. *Remote Sensing of Environment*, *37*(1), 35–46. https://doi.org/10.1016/0034-4257(91)90048-B

Corbane, C., Faure, J.-F., Baghdadi, N., Villeneuve, N., & Petit, M. (2008). Rapid Urban Mapping Using SAR/Optical Imagery Synergy. *Sensors*, *8*(12), 7125–7143. https://doi.org/10.3390/s8117125

Costanza, R., D 'arge, R., De Groot, R., Farber, S., Grasso, M., Hannon, B., … Van Den Belt, M. (1998). The value of the world's ecosystem services and natural capital. *Ecological Economics*, *25*(387), 3–15. Retrieved from http://www1.montpellier.inra.fr/lameta/articles/5.3.1_COSTANZA.pdf

Csillik, O., & Belgiu, M. (2017). Cropland mapping from Sentinel-2 time series data using object-based image analysis. *AGILE 2017*. Retrieved from https://agile-online.org/conference_paper/cds/agile_2017/shortpapers/127_ShortPaper_in_PDF.pdf

Cui, B., Yang, Q., Yang, Z., & Zhang, K. (2009). Evaluating the ecological performance of wetland restoration in the Yellow River Delta, China. *Ecological Engineering*, *35*(7), 1090–1103. https://doi.org/10.1016/j.ecoleng.2009.03.022

DeFries, R., Hansen, M., & Townshend, J. (1995). Global discrimination of land cover types from metrics derived from AVHRR pathfinder data. *Remote Sensing of Environment*, *54*(3), 209–222. https://doi.org/10.1016/0034-4257(95)00142-5

Defries, R. S., & Townshend, J. R. G. (1994). NDVI-derived land cover classifications at a global scale. *International Journal of Remote Sensing*, *15*(17), 3567–3586. https://doi.org/10.1080/01431169408954345

Demers, A. M., Banks, S. N., Pasher, J., Duffe, J., & Laforest, S. (2015). A Comparative Analysis of Object-Based and Pixel-Based Classification of RADARSAT-2 C–Band and Optical Satellite Data for Mapping Shoreline Types in the Canadian Arctic. *Canadian Journal of Remote Sensing*, *41*(1), 1–19. https://doi.org/10.1080/07038992.2015.1020361

Dennison, P. E., & Roberts, D. A. (2003). The effects of vegetation phenology on endmember selection and species mapping in southern California chaparral. *Remote Sensing of Environment*, *87*(2–3), 295–309. https://doi.org/10.1016/J.RSE.2003.07.001

Dennison, W. C., Orth, R. J., Moore, K. A., Stevenson, J. C., Carter, V., Kouar, S., … Batiuk, R. A. (1993). Assessing Water Quality with Submersed Aquatic Vegetation. *Bioscience*, 86–94. Retrieved from https://pdfs.semanticscholar.org/96b2/7f92413cdeb4b0f600d4c2f6af497f68ecc2.pdf

Estes, J. A., Terborgh, J., Brashares, J. S., Power, M. E., Berger, J., Bond, W. J., … Wardle, D. A. (2011). Trophic Downgrading of Planet Earth. *Science*, *333*(6040). Retrieved from http://science.sciencemag.org/content/333/6040/301

Foody, G. M. (2002). Status of land cover classification accuracy assessment. *Remote Sensing of Environment*, *80*(1), 185–201. https://doi.org/10.1016/S0034-4257(01)00295-4

Fu, B., Wang, Y., Campbell, A., Li, Y., Zhang, B., Yin, S., … Jin, X. (2017). Comparison of object-based and pixel-based Random Forest algorithm for wetland vegetation mapping using high spatial resolution GF-1 and SAR data. *Ecological Indicators*, *73*, 105–117. https://doi.org/10.1016/j.ecolind.2016.09.029

Furtado, L. F. de A., Silva, T. S. F., & Novo, E. M. L. de M. (2016). Dual-season and full-polarimetric C band SAR assessment for vegetation mapping in the Amazon várzea wetlands. *Remote Sensing of Environment*, *174*, 212–222. https://doi.org/10.1016/J.RSE.2015.12.013

Gandhi, G. M., Parthiban, S., Thummalu, N., & Christy, A. (2015). Ndvi: Vegetation Change Detection Using Remote Sensing and Gis – A Case Study of Vellore District. *Procedia Computer Science*, *57*, 1199–1210. https://doi.org/10.1016/J.PROCS.2015.07.415

Gilmore, M. S., Wilson, E. H., Barrett, N., Civco, D. L., Prisloe, S., Hurd, J. D., & Chadwick, C. (2008). Integrating multi-temporal spectral and structural information to map wetland vegetation in a lower Connecticut River tidal marsh. *Remote Sensing of Environment*, *112*(11), 4048–4060. https://doi.org/10.1016/J.RSE.2008.05.020

Giri, C., Ochieng, E., Tieszen, L. L., Zhu, Z., Singh, A., Loveland, T., … Duke, N. (2011). Status and distribution of mangrove forests of the world using earth observation satellite data. *Global Ecology and Biogeography*, *20*(1), 154–159. https://doi.org/10.1111/j.1466-8238.2010.00584.x

Gómez, C., White, J. C., & Wulder, M. A. (2016). Optical remotely sensed time series data for land cover classification: A review. *ISPRS Journal of Photogrammetry and Remote Sensing*, *116*, 55–72. https://doi.org/10.1016/j.isprsjprs.2016.03.008

Guerschman, J. P., Paruelo, J. M., Bella, C. Di, Giallorenzi, M. C., & Pacin, F. (2003). Land cover classification in the Argentine Pampas using multi-temporal Landsat TM data. *International Journal of Remote Sensing*, *24*(17), 3381–3402. https://doi.org/10.1080/0143116021000021288

Guyot, G. (1990). Optical properties of vegetation canopies. *Optical Properties of Vegetation Canopies.*, 19–43. Retrieved from https://www.cabdirect.org/cabdirect/abstract/19920753700

Haas, J., & Ban, Y. (2014). Urban growth and environmental impacts in Jing-Jin-Ji, the Yangtze, River Delta and the Pearl River Delta. *International Journal of Applied Earth Observation and Geoinformation*, *30*, 42–55. https://doi.org/10.1016/j.jag.2013.12.012

Halabuk, A., & Mojses, M. (2015). Using of MODIS NDVI Time Series for Grassland Habitat Classification and Assessment. *VEGA*. Retrieved from http://rsgis4hq.geo.tuwien.ac.at/fileadmin/editors/RSGIS4HQ/proceedings/RSGIS4HQ_Halabuk.pdf

Han, M., & Yu, H. (2016). Wetland dynamic and ecological compensation of the Yellow River Delta based on RS. *Energy Procedia*, *104*, 129–134. https://doi.org/10.1016/j.egypro.2016.12.023

Hardisky, M. A., Klemas, V., & Gross, M. F. (1986). Remote sensing of coastal wetlands. Retrieved from https://ntrs.nasa.gov/search.jsp?R=19870053670

He, C., Zhang, Q., Li, Y., Li, X., & Shi, P. (2005). Zoning grassland protection area using remote sensing and cellular automata modeling—A case study in Xilingol steppe grassland in northern China. *Journal of Arid Environments*, *63*(4), 814–826. https://doi.org/10.1016/j.jaridenv.2005.03.028

Hess, L. L., Melack, J. M., Filoso, S., & Yong Wang. (1995). Delineation of inundated area and vegetation along the Amazon floodplain with the SIR-C synthetic aperture radar. *IEEE Transactions on Geoscience and Remote Sensing*, *33*(4), 896–904. https://doi.org/10.1109/36.406675

Hess, L. L., Melack, J. M., & Simonett, D. S. (1990). Radar detection of flooding beneath the forest canopy: a review. *International Journal of Remote Sensing*, *11*(7), 1313–1325. https://doi.org/10.1080/01431169008955095

Horritt, M. S., Mason, D. C., Cobby, D. M., Davenport, I. J., & Bates, P. D. (2003). Waterline mapping in flooded vegetation from airborne SAR imagery. *Remote Sensing of Environment*, *85*(3), 271–281. https://doi.org/10.1016/S0034-4257(03)00006-3

Immitzer, M., Vuolo, F., & Atzberger, C. (2016). First Experience with Sentinel-2 Data for Crop and Tree Species Classifications in Central Europe. *Remote Sensing*, *8*(3), 166. https://doi.org/10.3390/rs8030166

Jackson, J. B. C., Kirby, M. X., Berger, W. H., Bjorndal, K. A., Botsford, L. W., Bourque, B. J., … Warner, R. R. (2001). Historical Overfishing and the Recent Collapse of Coastal Ecosystems. *Science*, *293*(5530). Retrieved from http://science.sciencemag.org/content/293/5530/629

Jennings, M., Loucks, O., Glenn-Lewin, D., Peet, R., Faber-Langendoen, D., Grossman, D., … Hidinger, L. (2003). Guidelines for describing associations and alliances of the U.S. national vegetation classification. Retrieved from http://vegbank.org/vegdocs/panel/esa_guidelines_v2.pdf

Judd, C., Steinberg, S., Shaughnessy, F., & Crawford, G. (2007). Mapping salt marsh vegetation using aerial hyperspectral imagery and linear unmixing in Humboldt Bay, California. *Wetlands*, *27*(4), 1144–1152. https://doi.org/10.1672/0277-5212(2007)27[1144:msmvua]2.0.co;2

Karlson, M., Ostwald, M., Reese, H., Sanou, J., Tankoano, B., & Mattsson, E. (2015). Mapping Tree Canopy Cover and Aboveground Biomass in Sudano-Sahelian Woodlands Using Landsat 8 and Random Forest. *Remote Sensing*, *7*(8), 10017–10041. https://doi.org/10.3390/rs70810017

Key, T. (2001). A Comparison of Multispectral and Multitemporal Information in High Spatial Resolution

Imagery for Classification of Individual Tree Species in a Temperate Hardwood Forest. *Remote Sensing of Environment*, *75*(1), 100–112. https://doi.org/10.1016/S0034-4257(00)00159-0

Klemas, V. (2001). Remote sensing of landscape-level coastal environmental indicators. *Environmental Management*. Retrieved from http://www.springerlink.com/index/HH5WRNYM3T11YGH2.pdf

Kokaly, R. F., Despain, D. G., Clark, R. N., Eric Livo, K., & Eric, K. (2003). Mapping vegetation in Yellowstone National Park using spectral feature analysis of AVIRIS data. Retrieved from http://digitalcommons.unl.edu/usgsstaffpub

Kokaly, R. F., Despain, D. G., Clark, R. N., & Livo, K. E. (2003). Mapping vegetation in Yellowstone National Park using spectral feature analysis of AVIRIS data. *Remote Sensing of Environment*, *84*(3), 437–456. https://doi.org/10.1016/S0034-4257(02)00133-5

Kong, D., Miao, C., Borthwick, A. G. L., Duan, Q., Liu, H., Sun, Q., … Gong, W. (2015). Evolution of the Yellow River Delta and its relationship with runoff and sediment load from 1983 to 2011. *Journal of Hydrology*, *520*, 157–167. https://doi.org/10.1016/J.JHYDROL.2014.09.038

Kumar, P., Prasad, R., Gupta, D. K., Mishra, V. N., Vishwakarma, A. K., Yadav, V. P., … Avtar, R. (2017). Estimation of winter wheat crop growth parameters using time series Sentinel-1A SAR data. *Geocarto International*, 1–15. https://doi.org/10.1080/10106049.2017.1316781

Le Toan, T., Laur, H., Mougin, E., & Lopes, A. (1989). Multitemporal and dual-polarization observations of agricultural vegetation covers by X-band SAR images. *IEEE Transactions on Geoscience and Remote Sensing*, *27*(6), 709–718. https://doi.org/10.1109/TGRS.1989.1398243

Lee, K. H. (1991). *Wetlands detection methods investigation*. (R.S. lunetta, Ed.). Las Vegas: United States Environmental Protection Agency.

Lee, K., & Lunetta, R. (1995). Wetland detection methods. *JG Lyon, and J. McCarthy. Eds, Wetland and*. Retrieved from https://scholar.google.com/scholar_lookup?title=Wetland Detection Methods&author=K.H.. Lee&author=R.S.. Lunetta&pages=249-284&publication_year=1996

Li, J., & Chen, W. (2005). A rule-based method for mapping Canada's wetlands using optical, radar and DEM data. *International Journal of Remote Sensing*, *26*(22), 5051–5069. https://doi.org/10.1080/01431160500166516

Li, J., Peng, S., & Li, Z. (2017). Detecting and attributing vegetation changes on China's Loess Plateau. *Agricultural and Forest Meteorology*, *247*, 260–270. https://doi.org/10.1016/J.AGRFORMET.2017.08.005

Li, S., Cui, B., Xie, T., Shao, X., & Zhang, M. (2016). Consequences and Implications of Anthropogenic Desalination of Salt Marshes on Macrobenthos. *CLEAN - Soil, Air, Water*, *44*(1), 8–15. https://doi.org/10.1002/clen.201400787

Li, S., Wang, G., Deng, W., Hu, Y., & Hu, W.-W. (2009). Influence of hydrology process on wetland landscape pattern: A case study in the Yellow River Delta. *Ecological Engineering*, *35*(12), 1719–1726. https://doi.org/10.1016/J.ECOLENG.2009.07.009

Li, Y. F., Huang, Y. L., & Li, S. K. (1991). A primarily analysis on the coastal physiognomy and deposition of the modern Yellow River Delta. *Acta Oceanol Sin*, *13*(5), 662–671. Retrieved from https://www.scopus.com/record/display.uri?eid=2-s2.0-84875254781&origin=inward&txGid=49491faa20b342734398e6ddaaa7e256

Liu, Y., Liu, J., & Chen, Y. (2017). Research on distribution patterns and population structure of Tamarix Chinensis in the intertidal zone of coastal wetlands in Yellow River Delta. *Ecological Science*, *36*(1), 153–158.

Lobato, C. M. C., Soares, B. E., Begot, T. O. R., & Montag, L. F. de A. (2016). Tidal pools as habitat for juveniles of the goliath grouper Epinephelus itajara (Lichtenstein 1822) in the Amazonian coastal zone, Brazil. *Natureza & Conservação*, *14*(1), 20–23. https://doi.org/10.1016/j.ncon.2015.12.001

Lu, D., & Weng, Q. (2007). A survey of image classification methods and techniques for improving classification performance. *International Journal of Remote Sensing*, *28*(5), 823–870. https://doi.org/10.1080/01431160600746456

Ma, T., Liang, C., & Li, X. (2015). Quantitative assessment of impacts of reclamation activities on coastal wetlands in China. *Wetland Science*, *13*(6), 653–659.

Malthus, T. J., & George, D. G. (1997). Airborne remote sensing of macrophytes in Cefni Reservoir, Anglesey, UK. *Aquatic Botany*, *58*(3–4), 317–332. https://doi.org/10.1016/S0304-3770(97)00043-0

Martinez, J., & Letoan, T. (2007). Mapping of flood dynamics and spatial distribution of vegetation in the Amazon floodplain using multitemporal SAR data. *Remote Sensing of Environment*, *108*(3), 209–223. https://doi.org/10.1016/j.rse.2006.11.012

Menge, B. ., & Branch, G. . (2001). Rocky intertidal communitites. In M. D. Bertness, S. D. (Steven D.

Gaines, & M. E. Hay (Eds.), *Marine community ecology* (pp. 221–251). Sinauer Associates. Retrieved from http://www.vliz.be/en/imis?module=ref&refid=99190&printversion=1&dropIMIStitle=1

Millard, K., & Richardson, M. (2013). Wetland mapping with LiDAR derivatives, SAR polarimetric decompositions, and LiDAR–SAR fusion using a random forest classifier. *Canadian Journal of Remote Sensing*, *39*(4), 290–307. https://doi.org/10.5589/m13-038

Nageswara Rao, P. P., Shobha, S. V., Ramesh, K. S., & Somashekhar, R. K. (2005). Satellite-based assessment of agriculture drought in Karnatake State. *@ Photonirvachak Journal of the Indian Society of Remote Sensing*, *33*(3). Retrieved from https://www.researchgate.net/profile/P_P_Rao/publication/225508641_Satellite-based_assessment_of_agricultural_drought_in_Karnataka_State/links/58ce0e934585157b6dae6ba5/Satellite-based-assessment-of-agricultural-drought-in-Karnataka-State.pdf

Onaindia, M., de Bikuña, B. G., & Benito, I. (1996). Aquatic Plants in Relation to Environmental Factors in Northern Spain. *Journal of Environmental Management*, *47*(2), 123–137. https://doi.org/10.1006/jema.1996.0041

Ortega-Morales, B. O., Chan-Bacab, M. J., De la Rosa-García, S. del C., & Camacho-Chab, J. C. (2010). Valuable processes and products from marine intertidal microbial communities. *Current Opinion in Biotechnology*, *21*(3), 346–352. https://doi.org/10.1016/j.copbio.2010.02.007

Ottinger, M., Kuenzer, C., Liu, G., Wang, S., & Dech, S. (2013). Monitoring land cover dynamics in the Yellow River Delta from 1995 to 2010 based on Landsat 5 TM. *Applied Geography*, *44*, 53–68. https://doi.org/10.1016/j.apgeog.2013.07.003

Ozesmi, S. L., & Bauer, M. E. (2002). Satellite remote sensing of wetlands. *Wetlands Ecology and Management*, *10*(5), 381–402. https://doi.org/10.1023/A:1020908432489

Pal, M. (2005). Random forest classifier for remote sensing classification. *International Journal of Remote Sensing*. Retrieved from http://www.tandfonline.com/doi/abs/10.1080/01431160412331269698

Pang, G., Wang, X., & Yang, M. (2017). Using the NDVI to identify variations in, and responses of, vegetation to climate change on the Tibetan Plateau from 1982 to 2012. *Quaternary International*, *444*, 87–96. https://doi.org/10.1016/J.QUAINT.2016.08.038

Pellizzeri, T. M., Gamba, P., Lombardo, P., & Dell'Acqua, F. (2003). Multitemporal/multiband sar classification of urban areas using spatial analysis: statistical versus neural kernel-based approach. *IEEE Transactions on Geoscience and Remote Sensing*, *41*(10), 2338–2353. https://doi.org/10.1109/TGRS.2003.818762

Price, J. (1992). Variability of high-resolution crop reflectance spectra. *International Journal of Remote Sensing*. Retrieved from http://www.tandfonline.com/doi/abs/10.1080/01431169208904066

Qi, S., & Fang, L. (2009). Environmental Degradation in the Yellow River Delta, Shandong Province, China. *http://dx.doi.org/10.1579/0044-7447(2007)36[610:EDITYR]2.0.CO;2*. https://doi.org/10.1579/0044-7447(2007)36[610:EDITYR]2.0.CO;2

Quegan, S., Le Toan, T., Yu, J. J., Ribbes, F., & Floury, N. (2000). Multitemporal ERS SAR analysis applied to forest mapping. *IEEE Transactions on Geoscience and Remote Sensing*, *38*(2), 741–753. https://doi.org/10.1109/36.842003

Ramsar. (2013). Shandong Yellow River Delta Wetland | Ramsar Sites Information Service. Retrieved August 21, 2017, from https://rsis.ramsar.org/ris/2187

Räsänen, A., Rusanen, A., Kuitunen, M., & Lensu, A. (2013). What makes segmentation good? A case study in boreal forest habitat mapping. *International Journal of Remote Sensing*, *34*(23), 8603–8627. https://doi.org/10.1080/01431161.2013.845318

Reed, B. C., Brown, J. F., VanderZee, D., Loveland, T. R., Merchant, J. W., & Ohlen, D. O. (1994). Measuring phenological variability from satellite imagery. *Journal of Vegetation Science*, *5*(5), 703–714. https://doi.org/10.2307/3235884

Rog, S. M., Clarke, R. H., & Cook, C. N. (2017). More than marine: revealing the critical importance of mangrove ecosystems for terrestrial vertebrates. *Diversity and Distributions*, *23*(2), 221–230. https://doi.org/10.1111/ddi.12514

Rogan, J. (2004). Remote sensing for mapping and monitoring land-cover and land-use change—an introduction. *Progress in Planning*, *61*(4), 301–325. Retrieved from http://www.academia.edu/7301323/Remote_sensing_for_mapping_and_monitoring_land-cover_and_land-use_change_an_introduction

Sartori, L. R., Imai, N. N., Mura, J. C., Novo, E. M. L. M., & Silva, T. S. F. (2011). Mapping Macrophyte Species in the Amazon Floodplain Wetlands Using Fully Polarimetric ALOS/PALSAR Data. *IEEE Transactions on Geoscience and Remote Sensing*, *49*(12), 4717–4728.

https://doi.org/10.1109/TGRS.2011.2157972
Schmidt, K. S., & Skidmore, A. K. (2003). Spectral discrimination of vegetation types in a coastal wetland. *Remote Sensing of Environment*, *85*(1), 92–108. https://doi.org/10.1016/S0034-4257(02)00196-7
Sentinel Hub/Sinergise. (2016). Sentinel Monitoring. Retrieved January 25, 2018, from https://www.sentinel-hub.com/
Shang, X., & Chisholm, L. A. (2014). Classification of Australian Native Forest Species Using Hyperspectral Remote Sensing and Machine-Learning Classification Algorithms. *IEEE Journal of Selected Topics in Applied Earth Observations and Remote Sensing*, *7*(6), 2481–2489. https://doi.org/10.1109/JSTARS.2013.2282166
Shao, Y., Campbell, J. B., Taff, G. N., & Zheng, B. (2015). An analysis of cropland mask choice and ancillary data for annual corn yield forecasting using MODIS data. *International Journal of Applied Earth Observation and Geoinformation*, *38*, 78–87. https://doi.org/10.1016/j.jag.2014.12.017
Silva, T. S. F., Costa, M. P. F., Melack, J. M., & Novo, E. M. L. M. (2008). Remote sensing of aquatic vegetation: theory and applications. *Environ Monit Assess*, *140*, 131–145. https://doi.org/10.1007/s10661-007-9855-3
Simard, M., Saatchi, S. S., & De Grandi, G. (2000). The use of decision tree and multiscale texture for classification of JERS-1 SAR data over tropical forest. *IEEE Transactions on Geoscience and Remote Sensing*, *38*(5), 2310–2321. https://doi.org/10.1109/36.868888
Sinergise. (2017). Sentinel 2 EO Products | Sentinel. Retrieved August 15, 2017, from http://www.sentinel-hub.com/apps/wms/wms-parameters/EOproducts
Singh, R. P., Roy, S., & Kogan, F. (2003). Vegetation and temperature condition indices from NOAA AVHRR data for drought monitoring over India. *International Journal of Remote Sensing*, *24*(22), 4393–4402. https://doi.org/10.1080/0143116031000084323
Song, C. Y., Huang, C., Liu, Q. S., & Liu, G. H. (2010). Simulation for Suaeda heteroptera potential distribution in the Yellow River Delta by using generalized additive models. *J. Nat. Resour.*, *25*(4), 677–685.
Spanglet, H. J., Ustin, S. L., & Rejmankova, E. (1998). Spectral reflectance characteristics of California subalpine marsh plant communities. *Wetlands*, *18*(3), 307–319. https://doi.org/10.1007/BF03161526
Suhet. (2015). Sentinel-2 User Handbook. *ESA Standard Document*, (1), 64. Retrieved from https://sentinel.esa.int/documents/247904/685211/Sentinel-2_User_Handbook
Sun, W., Sun, Z., Tian, L., & Hu, X. (2017). Variation and prediction of different marsh landscapes in intertidal zone of the Yellow River Delta. *Acta Ecologica Sinica*, *37*(1). https://doi.org/10.5846/stxb201607261524
Sun, Z., Mou, X., Tong, C., Wang, C., Xie, Z., Song, H., … Lv, Y. (2015). Spatial variations and bioaccumulation of heavy metals in intertidal zone of the Yellow River estuary, China. *CATENA*, *126*, 43–52. https://doi.org/10.1016/j.catena.2014.10.037
Swennen, C., Duiven, P., & Spaans, A. L. (1982). Numerical density and biomass of macrobenthic animals living in the intertidal zone of Surinam, South America. *Netherlands Journal of Sea Research*, *15*(3–4), 406–418. https://doi.org/10.1016/0077-7579(82)90067-9
Tang, Z., Ma, J., Peng, H., Wang, S., & Wei, J. (2017). Spatiotemporal changes of vegetation and their responses to temperature and precipitation in upper Shiyang river basin. *Advances in Space Research*, *60*(5), 969–979. https://doi.org/10.1016/J.ASR.2017.05.033
Toll, D. L. (1985). Analysis of digital LANDSAT MSS and SEASAT SAR data for use in discriminating land cover at the urban fringe of Denver, Colorado. *International Journal of Remote Sensing*, *6*(7), 1209–1229. https://doi.org/10.1080/01431168508948273
Torbick, N., Chowdhury, D., Salas, W., & Qi, J. (2017). Monitoring rice agriculture across myanmar using time series Sentinel-1 assisted by Landsat-8 and PALSAR-2. *Remote Sensing*, *9*(2). https://doi.org/10.3390/RS90201019
Torres, R., Snoeij, P., Geudtner, D., Bibby, D., Davidson, M., Attema, E., … Rostan, F. (2012). GMES Sentinel-1 mission. *Remote Sensing of Environment*, *120*, 9–24. https://doi.org/10.1016/j.rse.2011.05.028
Traganos, D., & Reinartz, P. (2017). Mapping Mediterranean seagrasses with Sentinel-2 imagery. *Marine Pollution Bulletin*. https://doi.org/10.1016/J.MARPOLBUL.2017.06.075
Tucker, C. J. (1979). Red and photographic infrared linear combinations for monitoring vegetation. *Remote Sensing of Environment*, *8*(2), 127–150. https://doi.org/10.1016/0034-4257(79)90013-0
Villa, P., Boschetti, M., Morse, J. L., & Politte, N. (2012). A multitemporal analysis of tsunami impact on coastal vegetation using remote sensing: a case study on Koh Phra Thong Island, Thailand. *Natural*

Hazards, *64*(1), 667–689. https://doi.org/10.1007/s11069-012-0261-y
Villa, P., Bresciani, M., Bolpagni, R., Pinardi, M., & Giardino, C. (2015). A rule-based approach for mapping macrophyte communities using multi-temporal aquatic vegetation indices. *Remote Sensing of Environment*, *171*(171), 218–233. https://doi.org/10.1016/j.rse.2015.10.020
Vis, C., Hudon, C., & Carignan, R. (2003). An evaluation of approaches used to determine the distribution and biomass of emergent and submerged aquatic macrophytes over large spatial scales. *Aquatic Botany*, *77*(3), 187–201. https://doi.org/10.1016/S0304-3770(03)00105-0
Vrieling, A., Skidmore, A. K., Wang, T., Meroni, M., Ens, B. J., Oosterbeek, K., … Paganini, M. (2017). Spatially detailed retrievals of spring phenology from single-season high-resolution image time series. *International Journal of Applied Earth Observation and Geoinformation*, *59*, 19–30. https://doi.org/10.1016/j.jag.2017.02.021
Wang, H., Bi, N., Saito, Y., Wang, Y., Sun, X., Zhang, J., & Yang, Z. (2010). Recent changes in sediment delivery by the Huanghe (Yellow River) to the sea: Causes and environmental implications in its estuary. *Journal of Hydrology*, *391*(3–4), 302–313. https://doi.org/10.1016/J.JHYDROL.2010.07.030
Wang, L., Han, Z., He, J., Wang, H., & Li, X. (n.d.). Recovering Design Patterns to Support Program Comprehension. Retrieved from http://delivery.acm.org/10.1145/2380000/2372248/p49-wang.pdf?ip=210.31.76.107&id=2372248&acc=ACTIVE SERVICE&key=BF85BBA5741FDC6E.6D8DAD7CEE0DF4B5.4D4702B0C3E38B35.4D4702B0C3E38B35&__acm__=1516758463_7cf09901d605a06122a08bcc9294c212
Waycott, M., Duarte, C. M., Carruthers, T. J. B., Orth, R. J., Dennison, W. C., Olyarnik, S., … Williams, S. L. (2009). Accelerating loss of seagrasses across the globe threatens coastal ecosystems. *Proceedings of the National Academy of Sciences of the United States of America*, *106*(30), 12377–81. https://doi.org/10.1073/pnas.0905620106
Yates, K. K., Rogers, C. S., Herlan, J. J., Brooks, G. R., Smiley, N. A., & Larson, R. A. (2014). Diverse coral communities in mangrove habitats suggest a novel refuge from climate change. *Biogeosciences*, *11*(16), 4321–4337. https://doi.org/10.5194/bg-11-4321-2014
Yuan, L., & Zhang, L. (2006). Identification of the spectral characteristics of submerged plant Vallisneria spiralis. *Acta Ecologica Sinica*, *26*(4), 1005–1010. https://doi.org/10.1016/S1872-2032(06)60019-X
Zhang, A., Yuan, X., Yang, X., Shao, S., Li, J., & Ding, D. (2016). Temporal and spatial distributions of intertidal macrobenthos in the sand flats of the Shuangtaizi Estuary, Bohai Sea in China. *Acta Ecologica Sinica*, *36*(3), 172–179. https://doi.org/10.1016/j.chnaes.2016.04.003
Zhang, X., & Li, P. (2006). Regional natural disaster risk of coastal wetland in Yellow River Delta. *Journal of Natural Disasters*, *15*(1), 159–164.
Zhao, S., Liu, X., Cheng, D., Liu, G., Liang, B., Cui, B., & Bai, J. (2016). Temporal–spatial variation and partitioning prediction of antibiotics in surface water and sediments from the intertidal zones of the Yellow River Delta, China. *Science of The Total Environment*, *569–570*, 1350–1358. https://doi.org/10.1016/j.scitotenv.2016.06.216